



European Union's Seventh Framework Programme

Grant Agreement N<sup>o</sup>: **603521**

Project Acronym: **PREFACE**

Project full title: **Enhancing prediction of tropical Atlantic climate and its impacts**

Instrument: Collaborative Project

Theme: ENV.2013.6.1-1 – *Climate-related ocean processes and combined impacts of multiple stressors on the marine environment*

Start date of project: 1 November 2013

Duration: 48 Months

**Deliverable reference number and full title:** D6.2. "*Diagnostic experiments of model drift*"

**Lead beneficiary for this deliverable:** Uni Research

**Due date of deliverable:** 31.10.2016

**Actual submission date:** 02.05.2017

Project co-funded by the European Commission within the Seven Framework Programme (2007-2013)		
Dissemination Level		
<b>PU</b>	Public	X
<b>PP</b>	Restricted to other programme participants (including the Commission Services)	
<b>RE</b>	Restricted to a group specified by the Consortium (including the Commission Services)	
<b>CO</b>	Confidential, only for members of the Consortium (including the Commission Services)	

**Contribution to project objectives** – with this deliverable, the project has contributed to the achievement of the following objectives (from Annex I / DOW, Section B1.1.):

N.º	Objective	Yes	No
1	Reduce uncertainties in our knowledge of the functioning of Tropical Atlantic (TA) climate, particularly climate-related ocean processes (including stratification) and dynamics, coupled ocean, atmosphere, and land interactions; and internal and externally forced climate variability.	X	
2	Better understand the impact of model systematic error and its reduction on seasonal-to-decadal climate predictions and on climate change projections.	X	
3	Improve the simulation and prediction TA climate on seasonal and longer time scales, and contribute to better quantification of climate change impacts in the region.		X
4	Improve understanding of the cumulative effects of the multiple stressors of climate variability, greenhouse-gas induced climate change (including warming and deoxygenation), and fisheries on marine ecosystems, functional diversity, and ecosystem services (e.g., fisheries) in the TA.		X
5	Assess the socio-economic vulnerabilities and evaluate the resilience of the welfare of West African fishing communities to climate-driven ecosystem shifts and global markets.		X

**Author(s) of this deliverable:** Toniazzo, T.<sup>1</sup>, Voltaire, A.<sup>2</sup>

<sup>1</sup> Uni Research, Bergen, Norway; <sup>2</sup> Météo-France, CNRM, Toulouse, France

### EXECUTIVE SUMMARY:

Diagnostic studies of bias development in seasonal hindcasts with initialized ensemble integrations of the climate models from the participating groups are summarized in Section 1. These served as a basis for the formulation and evaluation of a set of coordinated diagnostic hindcast sensitivity tests whereby simulated wind-stress was replaced in specified regions with observations-derived windstress fields. The analysis of results (Section 2) from individual models was mainly carried out by the corresponding modelling groups, but a unified analysis of common behaviour across models is presented here. The general conclusion is that model SST and precipitation biases are most sensitive to windstress over the equatorial Atlantic. The MF/CERFACS model shows sensitivity to coastal windstress; only NorESM (UiB/UniRes) shows sensitivity to the windstress away from the Equator and the coast. Further sensitivity tests carried out by individual modelling groups highlight particular aspects of model sensitivity (Section 3). One that appears consistently across the models is excess near-surface ocean stratification, which can be mitigated either via surface forcing (EC-Earth experiment) or via increased mixing by additional processes (near-inertial waves in NorESM).

**Contents**

<b>EXECUTIVE SUMMARY:</b> .....	2
<b>1. Introduction</b> .....	4
<b>2. Analysis of model systematic drift in tropical Atlantic</b> .....	4
2.1. Data and methods.....	4
2.2. General results on model drift in the tropical Atlantic and working hypotheses for coordinated hindcast sensitivity experiments (SEX) .....	7
<b>3. Coordinated hindcast sensitivity experiments</b> .....	11
3.1. Description of experiments.....	11
3.2. Control experiments .....	11
3.3. Wind-stress replacement experiments .....	12
3.4. Preliminary results from coordinated SEX .....	13
<b>4. Additional experiments</b> .....	13
4.1. EC-Earth.....	14
4.2. MF-CNRM - CERFACS.....	14
4.3. NorCPM.....	15
<b>REFERENCES</b> .....	16
<b>FIGURES</b> .....	18

## **1. Introduction**

This report documents progress in understanding and correcting systematic biases in numerical global-circulation models (GCMs) that affect seasonal-to-decadal hindcasts based on such models. When they are initialized with an observations-derived atmosphere-ocean state, GCM simulations start to drift away from the observed climatology towards the biased model-mean climatology. The spatial and temporal pattern of this drift is characteristic of each model – more so than the final biased mean state – and its analysis provides evidence for some of the mechanisms responsible for the model mean biases. Targeted model sensitivity experiments in hindcast mode and the resulting effects on hindcast drift allow to test such mechanisms and to focus model parametrization development or tuning effort towards better numerical climate forecasts and projections. WP6 within PREFACE is dedicated to this line of investigation. This Deliverable summarizes results on all three aspects, with the description and initial evaluation of a set of coordinate model sensitivity experiments between the participating groups as its centrepiece.

## **2. Analysis of model systematic drift in tropical Atlantic**

### **2.1. Data and methods**

The report is primarily based on two types of hindcast experiments. The first are standard hindcast experiments performed with participating models. An analysis for common period and start dates is presented in section 2, while general results from the individual groups are summarized in section 2.2. In the second set, hindcasts are repeated with surface winds being replaced by observation based estimates for selected regions to disentangle the impact of various wind errors on the development of mean forecast drift. These experiments are referred to as the coordinated hindcast sensitivity experiments (SEX), and are summarized in section 3.

#### **2.1.1. ECMWF System 4**

System 4 combines cycle 36R4 of the Integrated Forecast System (IFS) with version 3.0 of the Nucleus for European Modelling of the Ocean (NEMO). The atmosphere component IFS runs on a TL255 spectral grid, with grid point calculations made on an N128 Gaussian grid, giving a horizontal resolution of order  $0.7^\circ$ . It has 91 levels extending to a pressure level of 1 Pa. Ocean component NEMO uses a modified ORCA1 grid, which gives a resolution of about  $1^\circ$ , and has 42 vertical levels. The two models are coupled using a modified version of OASIS3, with coupling performed every three hours. For modifications to the model components in System 4, refer to Molteni et al (2011).

Before 2010 (and including the period of data we have provided for this study), the IFS is initialised from ERA-Interim reanalysis data (Dee et al, 2011) and NEMO is initialised from ORA-S4 data (Balmaseda et al, 2013), with sea-surface temperatures derived from the OISSTv2 product of Reynolds et al (2002).

Twenty-eight operational hindcasts from the System 4 archive were considered, one for each year between 1996 and 2009 with start dates on 1 February and 1 May. These hindcasts are seven months in duration and contain at least 15 ensemble members. For the purposes of analysing the model systematic drift, a subsample of eight members per forecast was used.

Reading and UniRes have analysed the systematic forecast bias in the tropical Pacific and the tropical Atlantic in System 4. No sensitivity experiments were performed, but additional insight into the respective role of ocean and atmosphere biases was obtained from a parallel set of hindcasts where SSTs were prescribed from observations.

### **2.1.2. EC-Earth**

The coordinated hindcast sensitivity experiments (hereafter SEX) were performed by BSC with EC-Earth v3. Systematic biases in the control hindcasts were analysed by WU and BSC, who also performed additional sensitivity experiments in forecast mode. Valuable insights into model drift have also been obtained from the analysis by UniRes, partly in coordination with the analysis of ECMWF System 4 at Reading, of an older set of seasonal forecasts with EC-Earth version 2.3, also computed at BSC. EC-Earth v2 (Hazeleger et al. 2010, 2012) is based on cycle 31R1 (identical with ERA-Interim) of the Integrated Forecast System (IFS), coupled via OASIS3 (Valcke 2013) with version 2 of the Nucleus for European Modeling of the Ocean (NEMO; Madec 2008) with local ECMWF modifications and EC-EARTH developments. The IFS configuration has a horizontal resolution of TL159 (which corresponds to a 1.125 degree spacing (125 km) on a reduced N80 Gaussian grid) and 62 hybrid sigma-p levels in the vertical with a model top at 5 hPa. NEMO is used in the ORCA1 configuration with a nominal horizontal resolution of 1 degree with refinement at the equator, and 42 levels in the vertical. The drift analysis in the control integration was based on a set of four-month ensemble forecasts of Ec-Earth model for 1981-2000.

EC-Earth v3 is based on EC-Earth v2 with updated atmosphere, ocean, sea ice, and aerosol components. It uses the NEMO/ORCA1 at version 3.3 with 46 vertical levels (Madec et al. 2011) and the IFS at cycle 36r4 at T255 triangular truncation and 91 vertical levels (Riddaway, Newsletter ECMWF 2010). Data were analysed from a series of four-month long, five-member ensemble hindcasts initialised on 1 February and 1 May for each year between 2000-2009 using ORA-S4 for the ocean, ERA-Interim for the atmosphere, and the IC3 sea-ice analysis (Guemas et al. 2014). Both in terms of model and initialisation, the EC-Earth v3 hindcasts are thus very similar to ECWMF System 4.

### **2.1.3. MF CNRM-CM5**

CNRM-CM5 is the CMIP5 version of CNRM-CM, fully described in Voltaire et al. (2013). It is composed of the atmospheric model ARPEGE-Climat V5.2, and the ocean model NEMO 3.2. The atmospheric resolution is  $\sim 1.4^\circ$  (T127) and there are 31 vertical levels up to 10hPa. The ocean is based on an ORCA1 grid with 42 vertical levels. The coupling frequency is 1 day.

The control integration consists of three members over the period 1993-2009 for February and May starts. Hindcasts, including SEX, are initialised from the ECMWF reanalysis products, ERA-Interim for the atmosphere and ORA-S4 for the ocean.

### **2.1.4. CERFACS CM5**

CERFACS participated in SEX with a High-Resolution (HR) version of the CNRM-CM model that includes the atmospheric model ARPEGE-Climat (v5.3, differences with the 5.2 version used in the low resolution version - LR- are only related to bugfixes) in its T359L31 configuration ( $\sim 50$ km horizontal resolution) in the atmosphere. The version of the ocean model NEMO is v3.4 (improved physics and diagnostics compared to v3.2), running on an ORCA025L75 grid configuration. It corresponds to an increase in horizontal resolution in both components and an increase in ocean vertical resolution. The coupling time step is reduced

compared to the LR version to 3 hours. A description of the HR version can be found in Monerie et al. (2017).

As for the low resolution version, the control integration consists of three-members and 2 start dates but hindcasts are extended to seven-months. The hindcasts were full-field initialized from ERA-Interim for the atmosphere as the LR, whereas the high-resolution Glorys2V3 ocean reanalysis (Ferry et al. 2010) was used for ocean initialisation since it shares the same grid as the ocean component. To assess the role of the initial conditions, control integrations with the LR model have been performed starting from the same Glorys dataset. To properly initialise the LR version from Glorys, a LR ocean forced simulation nudged towards the Glorys reanalysis previously interpolated on the ORCA1L42 grid has been run over the period 1993-2009 to built pseudo-initial conditions. Finally the LR model is initialised from this ocean nudged simulation.

### **2.1.5. NorESM**

Control and SEX hindcasts were performed with the medium-resolution NorESM1-ME (Tjiputra et al., 2013), in the NorCPM configuration described in Counillon et al. (2016) and with a similar initialisation method. NorESM1-ME is based on the CESM version 1.0.3 (CESM1, Vertenstein et al., 2012). The atmosphere is based on the Community Atmosphere Model v4 (CAM4, Neale et al., 2010) with the finite-volume dynamical core on a regular 1.9x2.5 degree latitude-longitude grid and 26 hybrid sigma-p layers in the vertical. The physical parametrisation is modified with the addition of advanced aerosol physics and chemistry (Kirkevåg et al., 2013). The ocean component (Bentsen et al., 2012) is an updated version of the Miami isopycnal coordinate ocean model (MICOM, Bleck et al., 1992), with a horizontal resolution of approximately 1° on a curvilinear (displaced-pole) grid and 51 isopycnal (mass) layers in the vertical, with 2 additional layers representing a bulk mixed layer.

The initialisation employs an Ensemble Kalman Filter (EnKF) data assimilation scheme as in Counillon et al. (2016), except that the total rather than anomalous SST are assimilated. The observed SST is used to update the entire water column below for all ocean model variables. The ocean analysis assimilates the observations once monthly at the middle of each month and their associated covariance matrix is used to estimate a new ensemble of model states. In the atmosphere, the state variables (U, V, T) above the PBL of the model are nudged towards ERA-Interim reanalysis with a ten-day relaxation time-scale. This relaxation is applied up to the nominal start date of the forecast. The EnKF method is suboptimal in the presence of large model biases, and NorCPM displays a large forecast drift. The relatively weak atmospheric nudging only partially counteract this. At the nominal start dates of 1 February, 1 May the model has therefore already accumulated drift for approximately 15 days and the initial model state has a noticeable bias.

### **2.1.6 IPSL**

IPSL has also performed the control and SEX but an initial analysis shows that their initialisation method was not adequate for the purpose of the project. They are currently improving their initialisation method.

## **2.2. General results on model drift in the tropical Atlantic and working hypotheses for coordinated hindcast sensitivity experiments (SEX)**

For the coordinated analysis, we have only analysed the common period to all model integrations 2000-2009 and only three members are retained for the map plots whereas all members are used for daily time series plots in order to limit the noise.

As noted in previous work (e.g. Richter and Xie, 2008; Toniazzo and Woolnough, 2013; Richter, 2015), a warm bias in the eastern tropical Atlantic along the Equator and along the coast of southern Africa is a common feature among climate models. Figures 1 and 2 show this fact clearly for the control hindcasts. While the SST bias pattern shares common features among the models, their amplitude and time evolution vary greatly (Figures 1 to 4). However it is noted that the rate of bias growth tends to be greatest in late boreal Spring. Equally common in GCM are precipitation biases, with a generally dry bias over the tropical landmass of South America and the development of a spurious oceanic ITCZ-like band of precipitation south of the Equator in the Atlantic during boreal Spring (Figures 3 to 6). Concomitant surface wind biases are seen, which are generally westerly (eastward stress acting on the sea surface) in the West Atlantic over or near the Equator, again with an enhancement in late boreal Spring (Figure 7). Along the south-western coast of Africa, a region of oceanic upwelling where warm SST biases are prominent, the driving southerly wind-stress is weak in some models (MF-CNRM, NorESM) but not in others (Figure 8). Surface forcing by heat fluxes (Figure 9; positive downward) also is not generally biased positive in the regions with warm biases.

In the next subsections we provide a more detailed summary of results for individual models from analyses carried out independently by participating groups. Section 2.1 indicates that some models used by the participating groups in SEX are closely related with each other. This is borne out by the results of the systematic drift and bias analysis. Accordingly, we shall summarise results by different model “families”.

### **2.2.1. EC-Earth and ECMWF System 4**

The EC-Earth v3.1 and ECMWF System 4 exhibit a weaker warm bias in the eastern tropical Atlantic compared to other models (Figures 1 and 2).

System 4 shows elements of many of the common systematic biases found in the tropical Atlantic in modern GCMs. There is a weak cold tongue bias on the equator that persists for most of the year, along with a warm SST bias off the coast of southwestern Africa in the region dominated by marine stratocumulus. Through May and June, this warm bias spreads northwards and into the cold tongue region, reversing the sign of the SST here for a few months, before the cold error returns in July and August. The cold tongue suppresses rainfall on the equator, resulting in a double ITCZ bias in the Atlantic through much of the year. The model generally produces too much rainfall in the ITCZ, and is most anomalously wet in May, when a wet bias spans much of the tropical Atlantic, with much of the excess rain falling in the southern branch of the ITCZ. Also of note is the low-level wind bias, which tends to be easterly through much of the year (implying that the model’s easterly trade winds are too strong). From March into April, however, there is a sharp flip in sign of this wind bias from easterly to westerly (implying that the trade winds suddenly become too weak). This error develops off the coast of South America and spreads across the entire basin, before fading

in magnitude and drifting north, eventually being replaced by the easterly (too strong) biases by July and August. It is visible also in uncoupled (prescribed-SST) hindcasts.

A set of four-month ensemble forecasts of EC-Earth v2 model for 1981-2000 was used to investigate the evolution and causes of the coupled model biases over tropical/subtropical Atlantic sector. The four month integration from the four initial states (February, May, August and November) covers all the seasons and provides an opportunity to study the seasonal dependence of the evolution of systematic biases. A focus was placed on boreal Spring as the season when the strongest bias development occurs.

There appears a cold bias in the equatorial Atlantic, extending from Gulf of Guinea to the western equatorial Atlantic, during most of the year. However, the model fails to reproduce the boreal summer cold tongue, resulting in a reinforced spurious zonal SST gradient along the equator similar to that observed over most of the CMIP models (Davey et al., 2002). Precipitation biases tend to develop quickly in the first month of the forecast in both February and May start dates. The model tends to produce excess rainfall south of the equator leading to a southward shift of the ITCZ during Spring. Also evident is a dry bias over north-eastern Brazil. A number of factors that seem to be significant for the development of westerly bias over equatorial Atlantic have been identified and are being investigated. Most evident is its strong seasonal dependence, whereby the westerly bias initially appears in April in the February hindcast while developing immediately in the May hindcast. For the same validity time, the drift (i.e. bias time increment) appears very similar in the two hindcast sets. This suggested that the root causes of the westerly bias during late Spring and Summer have a local mechanistic origin that is not sensitive to global SST or circulation errors. The alternative hypothesis of a dry continent/wet ocean error as a driving cause is not supported by the similar results obtained from System 4, which has a much weaker and more localised dry continental bias but a similar wind phenomenology over the equatorial ocean.

Some of these results are documented in Shonk et al (2017, *Clim. Dyn.*, in press); another paper is in preparation.

WU analysed the physical mechanism of model drift in EC-Earth3.1 seasonal hindcasts. Tropical Atlantic climate is largely governed by strong air-sea coupling. They have investigated feedbacks between ocean vertical mixing, sea surface temperature (SST), cloud cover, and incident solar radiation at the surface (SSR) focussing on two regions: underneath the ITCZ and off the Angolan-Namibian coast. These regions suffer from positive SST biases that establish quickly (Fig. A).

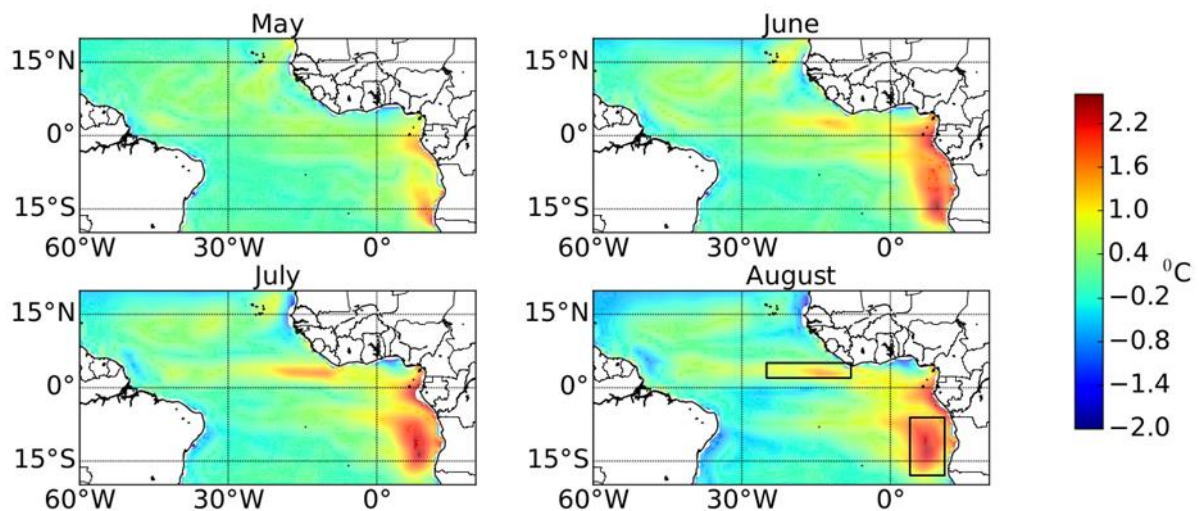


**Figure A:** SST bias of the EC-Earth3.1 hindcast fully initialised at the first of May with respect to ERA-Interim. The black boxes define the ITCZ region (25W-8W,2N-5N) and the AB region (4E-11E,18S-6S).

From reanalysis data, we identify an ocean mixing – SST – cloud cover – SSR feedback by correlating SST with SSR (SST – cloud cover – SSR) and vertical temperature gradient of the upper ocean with SST (ocean mixing – SST). Underneath the ITCZ SST anomalies lead to cloud cover anomalies that dampen the initial SST anomaly. In the region off the Angolan-Namibian coast cloud cover anomalies enhance SST anomalies, leading to a positive feedback (Fig. B). The cloud cover anomaly influences SSR. The SSR anomaly closes the feedback loop by not only influencing SST, but by also affecting ocean stratification and thereby ocean vertical mixing. The feedback and its impact on the development of the initial bias is evaluated in EC-Earth3.1. It is investigated with a seasonal mixed layer heat budget. The difference between integrated EC-Earth3.1 and the reanalysis budgets shows that EC-Earth overestimates the damping capacity in the ITCZ region and underestimates the positive feedback in the AB region (see Q lines in Fig. C). Insufficient ocean vertical mixing leads to positive biases in the residual, artificially warming SSTs.

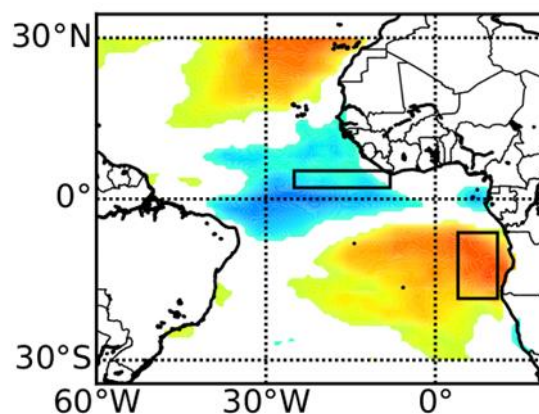


**Figure B:** Monthly anomaly correlation between SST and SSR from TropFlux reanalysis. Colours indicate the correlation coefficient ranging from -0.6 to 0.6.

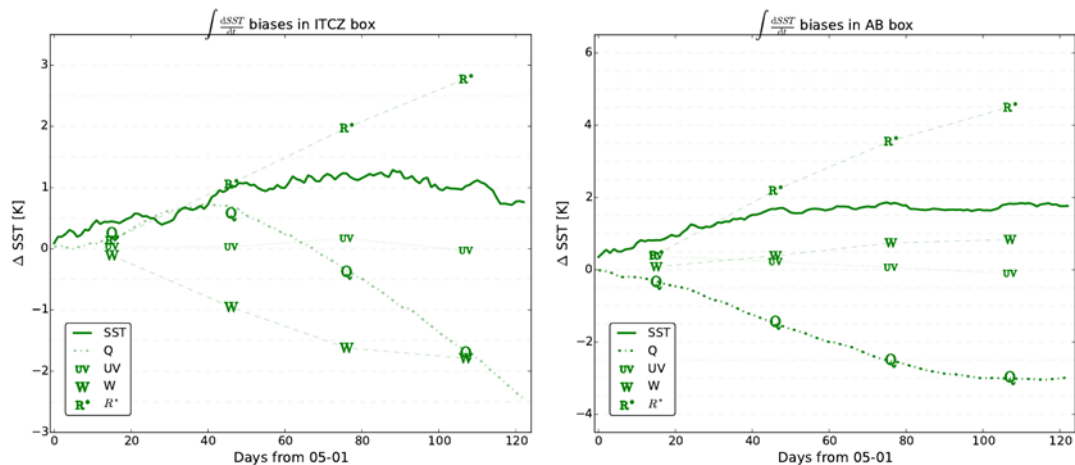


**Figure C:** Differences between the integrated heat budgets of EC-Earth3.1 and reanalysis data. UV are horizontal advection, W vertical advection, Q net heat flux forcing and R the residual.

The analysis has revealed that air-sea feedbacks play a significant role in the development of the initial drift. Our investigations show that in other CMIP5 models the feedbacks are incorrectly represented as well, which impacts their SST biases. A paper on this has been submitted to Journal of Climate (Deppenmeier, Haarsma and Hazeleger, “Ocean mixing – SST – cloud cover – shortwave radiation coupling in the tropical Atlantic”).

### 2.2.2. MF-CNRM and CERFACS

To analyse in details the processes associated with the SST bias development in the LR and HR versions of the CNRM-CM model, a heat budget analysis of the upper-ocean mixed layer was performed over the three boxes: equatorial box ATL3 (3°S-3°N, 20°W-0°) and two coastal boxes, ABA (25°S-15°S, 4°-width near-coastal fringe) and SBEN (34°S-25°S, 2°-width near-coastal fringe).

Comparison between the two versions suggests that increasing the resolution does not significantly reduce the SST biases in the equatorial Atlantic and SETA region and that, in general, similar processes are responsible for the SETA SST biases in the HR and LR versions.

In particular, analysis of the control integrations shows that the initial growth of the SST bias in ABA and SBEN, observed during the first 1.5-2 months, is likely associated with a local atmospheric forcing (weaker than observed wind stress and excessive solar radiation resulting from an underestimated low cloud cover). Further development of the SST bias is due to remote oceanic processes, in particular to an anomalous warm horizontal advection in the SETA from the Equator that penetrates southward of 25°S and is associated with the propagation along the coast of downwelling waves induced at the Equator by westerly wind bursts.

Comparison with a lower resolution (LR) version of the model suggests that increasing the resolution does not allow significantly improving the SST biases in the equatorial Atlantic and SETA region and that, in general, similar processes are responsible for the SETA SST biases in the HR and LR versions. However, a strong reduction of the biases in the HR

version in respect to the LR version is observed locally over the near-coastal Northern Benguela region and is due to better representation of fine-scale atmospheric and oceanic processes controlling the coastal upwelling. Overall, the results of the inter-comparison of the SETA SST bias evolution in the different hindcast experiments performed in this study (cf. Section 2 for the sensitivity experiments) can be interpreted in terms of the relative contributions of the warm horizontal advection, associated with equatorial forcing, and cold horizontal advection, associated with local offshore Ekman transport, to the regional mixed layer heat budget.

A scientific publication (Goubanova et al. in prep) with a detailed description of these results is in preparation.

### **2.2.3. NorCPM**

No analysis of the full-field initialised hindcasts with NorCPM has been performed yet, but some insight on the biases in the Angola-Benguela Frontal (ABF) Zone was obtained from sensitivity experiments in forced ocean (CORE) mode. They show a significant influence of the climatological wind-stress bias in the atmosphere component, responsible for about half of the large (~8 degree C) climatological bias in NorESM1-ME in this region. Roughly speaking, another 25% of the bias depends on surface heat fluxes, and the remaining bias stems from internal biases of the ocean model. These results are due to be published in Koseki et al. (2017).

## **3. Coordinated hindcast sensitivity experiments**

### **3.1. Description of experiments**

Five modelling centres (UREAD, UiB/UniRes, BSC/WU, MF-CNRM, CERFACS) have provided data from seasonal forecast experiments for the evaluation of the development of systematic biases in the respective models.

Four (UiB/UniRes, BSC/WU, MF-CNRM, CERFACS) centres participated in forecast sensitivity experiments whereby the simulated wind-stress was replaced with an observational estimate (ERA-Interim) to force the ocean in specified areas of the tropical Atlantic throughout for the duration of each forecast.

MF-CNRM collected data and produced summary plots for all the experiments. A first analysis of the results is presented here.

Two sets of hindcasts (for each model and for each experiment) with initialisation dates on 1st February and 1st May, respectively, are considered. A focus on boreal spring is justified from various studies (summarized above) that found both the largest biases and their most intense development during this time.

### **3.2. Control experiments**

The main results are summarised above for the individual models. In general, all models show fast development of systematic biases in the atmospheric wind field, on submonthly time-scales, independent of underlying SST biases. These are particularly evident in the tropical Atlantic sector for the May initialisation date, when associated regional precipitation biases are also observed, in a general wet ocean/dry land pattern, with especial intensification over and just south of the Equator. Westerly wind biases tend to develop thus

in the western equatorial Atlantic, and excess precipitation in the Atlantic 3 (20W-0, 5S-5N; ATL3) region. Further south, systematic warm biases develop along the western African coast, especially near the ABF.

As observed previously, the warm biases have different magnitudes but a common pattern emerges across models, with a warm eastern-Atlantic equatorial sector spreading along the coast. North of the ABF, warm biases are common to all models, irrespective of the local along-shore wind-stress biases. The diagnosed biases are both lead-time and seasonally dependent. However, from May onward, the atmospheric biases appear to develop in a qualitatively identical fashion in forecasts initialised in February and in forecasts initialised in May.

In other words, pre-existing global SST biases do not seem to exert a significant influence on the development of May-June wind and precipitation biases.

As noted above, SST biases vary significantly in amplitude between different model families. Precipitation biases, by contrast, are substantial in all cases.

### 3.3. Wind-stress replacement experiments

Although not necessarily the primary source of SST or precipitation bias in all the models, biased wind-stress forcing acting on the ocean, particularly over the Equator and along the coastal ocean of the south-eastern Atlantic, is a common problem and wind-stress sensitivity tests have therefore been selected for joint study by the modelling groups.

It was recognised that sensitivity tests with perturbed surface heat fluxes, which had also been originally envisaged, must necessarily be specifically targeted for each model separately, and face the additional difficulty of poorly constrained observational products.

Thus, three different forecast experiments were performed by the participating modelling centres (UiB/UniRes, MF-CNRM, CERFACS, BSC/WU). They are designed to target the areas where common systematic biases develop in the different forecast systems. Each experiment consists in replacing the simulated wind-stress field acting on the ocean model by the corresponding fields in the ERA-Interim dataset, in a different region for each experiment. These regions are (Figure D): the entire tropical Atlantic equatorward of 30 degree latitude (TAU30), the equatorial Atlantic only (5S-5N; TAUEQ), and the Angola-Benguela coast (10S-30S, 0°-coast; TAUBE).



**Figure D:** Regions of wind replacement in each sensitivity experiments

Each experiment was carried out for two sets of forecasts, with initialisation dates on 1st February and 1st May, respectively. An exception was made by Cerfacs, due to the high computational cost of the high-resolution integrations. Cerfacs decided to perform the sensitivity experiments for only the start date in February, as it showed stronger bias in the SETA relative to the hindcast starting in May.

### 3.4. Preliminary results from coordinated SEX

Figures 10-12 summarize the impact of wind-stress replacement on the evolution of SST biases in the four modelling systems. Filled areas on the plots highlight bias reductions. It can be seen that with TAU30 replacement a bias reduction is achieved in most hindcasts (Figure 10). The main exception is for EC-Earth v3, where improvements are only seen in the Atlantic 3 region (3S-3N, 20W-0), or in the Angola region (15S-3S, 10E-20E) from May onwards in the February hindcasts. Figure 3 details the nature of this error, which consists in insufficient SST cooling in the Angola sector compared with the observed seasonal cycle, associated with the spring intensification of the Angola Dome. The consistency of the developing warm bias with equatorial wind-stress biases however (Figure 7) suggests progressive thermocline deepening, associated with the combined equatorial-coastal waveguide as a possible driver for the Angola warm bias in EC-Earth (and, by similarity, in System 4).

This seems confirmed by comparison with the TAUEQ experiments, which show a similar impact as TAU30 in EC-Earth as well as in the MF-CNRM/CERFACS models. NorCPM, by contrast, displays significant additional sensitivity to off-equatorial wind-stress biases in the Angola and (even more) in the Benguela (32S-20S 12E-20E) sectors. This is consistent with the analysis of Koseki et al. (2017). NorCPM and MF-CNRM are the only models that show sensitivity to TAUBE replacement. The discrepancy between MF-CNRM and CERFACS depends primarily on the model resolution, whereby the meridional wind bias is substantially improved (Figure 8), and suggests that the higher wavenumbers in the spectral discretisation of the atmospheric model component are important for the representation of coastal winds. By contrast, ocean-model resolution does not seem to play a significant role locally (compare pink and yellow dashed lines in Figure 12). Considering the impacts on SSTs in the wider tropical Atlantic (Figures 13-18) does not add critical information to these conclusions. In these experiments, reduction in the warm biases over the Equatorial and eastern coastal Atlantic are accompanied by increased downward surface heat fluxes (Figures 18 and 19), which partly counteract the relative cooling. This confirms that, while surface fluxes contribute to SST errors in individual models in some areas, the response of ocean stratification and currents to biased wind-stress is a common driver of the warm SST errors across different models. Over the Equator, cooler conditions are accompanied by both increased short wave flux and reduced evaporation, while in the coastal areas the main response is from evaporation alone (Figures 21 and 22 ).

As mentioned earlier, while some models have a better representation of SSTs, biases in precipitation are ubiquitous and, correspondingly, models are more similar in their sensitivity in oceanic precipitation to surface wind forcing than in their sensitivity in SSTs (Figures 22-25). This may be understood in terms of different surface (SST-precipitation and precipitation-surface flux) feedbacks acting in different models (see Deppenmeier et al. 2017 for the case of EC-Earth): a large response in precipitation to changes in SSTs is typically accompanied by strong surface-flux damping of those SSTs. Note that such feedbacks are generally absent in the Benguela region, where the atmosphere is dry and stably stratified; unless warm-PBL biases are large enough for atmospheric stratification to become unstable and precipitation to occur as in the case of NorCPM (not shown).

## 4. Additional experiments

#### 4.1. EC-Earth

Sensitivity experiments performed with EC-Earth where the wind-stress is replaced with ERA-Interim winds show only a weak improvement in the warm bias (Fig. 10), implying that underestimated wind-stress is not the main driver of the east-Atlantic warm bias in EC-Earth. We assess here the impact of excessive solar penetration, caused by excessive solar fluxes and/or unrealistic solar penetration scheme, on the warm bias. The parameterization for solar penetration in NEMO follows the 2-waveband method of Lengaigne et al. (2007), with 58% of the solar radiation absorbed at the top few centimetres and the remaining 42% penetrating below the surface following an exponential profile at a length scale determined by the penetration depth. Here, we perform a sensitivity experiment where we increase solar penetration depth from 23m to 50m, which leads to less solar penetration to the oceanic mixed layer (experiment “SOL50”). We expect that increasing solar penetration depth will lead to a deeper and colder mixed layer, and a weaker warm SST bias in SOL50. However, the latent and longwave fluxes, which tend to cool and overcompensate the SST warming in the control simulation, are expected to decrease in magnitude in SOL50, thus reducing the magnitude of the cooling caused by the increased solar penetration depth. Results show that the warm bias is indeed reduced in SOL50 by about a third in magnitude in the forecasts initialized in May, while it is eradicated (and turned into a cold bias) in the forecasts initialized in November, implying that the warm bias is indeed linked to excessive solar penetration in the mixed layer in EC-Earth. The stronger response of the SST to the change in solar penetration in the boreal winter months suggests that seasonality in solar penetration, driven by the seasonality in biological activity in this region (Monger et al., 1997; Christian and Murtugudde, 2003), should be taken into account in the solar penetration schemes (Exarchou et al., 2016).

#### 4.2. MF-CNRM - CERFACS

Finally, given that the HR and LR models use different ocean-atmosphere coupling time-steps (3 hours and 1 day, respectively) we also tested the sensitivity of the SST bias development to coupling frequency. The corresponding sensitivity tests performed with the HR model indicated that the magnitude and evolution of the SST bias in the SETA and equatorial Atlantic regions during the period of the hindcasts are similar in case of 3h and 1day coupling.

The large wind biases found in CNRM-CM5 in the equatorial Atlantic have been shown to be already important in SST-prescribed atmospheric simulations. Thus, these biases are not only related to coupling feedbacks, but also to deficiencies in the atmospheric model. Consequently, the wind bias has been studied in SST-prescribed atmospheric simulations. A set of initialised atmospheric simulations, using the so-called Transpose-AMIP protocol, have been performed to disentangle the role of large-scale, remote errors and that of more local processes, related to the atmospheric parameterizations in establishing the wind biases. This equatorial wind bias develops within a few days and is associated with the regional precipitation biases, i.e. an underestimate of precipitation along the coast of South American coast and an excess of precipitation in Gulf of Guinea. The latter bias develops much slower than the first one and thus appears as a response of the large-scale circulation to other biases, especially to the lack of convective heating in the western equatorial Atlantic. A careful analysis of the water budget in this region indicates that convection is inactive there and that the total moisture convergence remains too weak. This is, related to an

underestimation of surface evaporation. As the CNRM-CM5 convective scheme closure is based on (resolved and sub-grid scale) moisture convergence, it is hypothesized that using a CAPE-type closure might reduce the precipitation biases and consequently the wind bias. This idea is supported by the recent study of Siongco et al (2017).

### 4.3. NorCPM

No further sensitivity tests were carried out in forecast mode; however, a promising development in NorESM1-ME has been shown by UCPH with the introduction of a parametrisation for near-inertial wave (NIW) mixing on the ocean surface. It is shown in particular that increased surface mixing improves the climatology of SSTs, wind and precipitation near the Equator with especially good results in the Atlantic. This work is documented in Pillar et al. (2017), to be submitted to Journal of Climate. Figure E in Pillar et al. (2017) is reproduced below. It shows the impact of additional mixing from NIW activity on NorESM model simulations. In the Atlantic in particular the wet and westerly bias south of the Equator is mitigated. As in the SEX, a concomitant mild reduction of SST biases in the south-eastern Atlantic occurs.

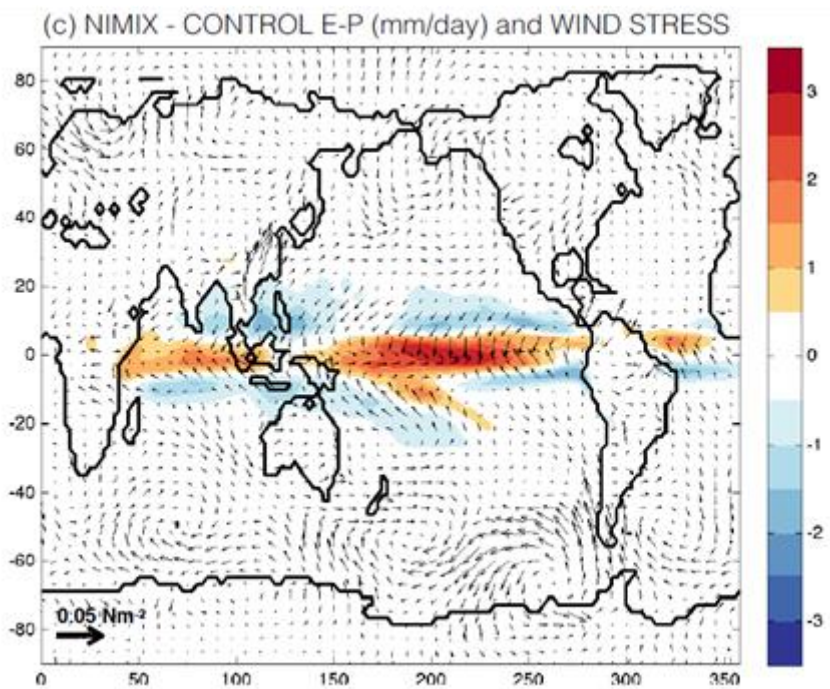


**Figure E:** Impacts of the NIW parameterisation on precipitation and wind stress.

## REFERENCES

- Bentsen M., Bethke I., Debernard J. B., Iversen T., Kirkevåg A., co-authors. The Norwegian Earth System Model, NorESM1-M – Part 1: description and basic evaluation. *Geosci. Model Dev. Discuss.* 2012; 5: 2843–2931. DOI: <http://dx.doi.org/10.5194/gmdd-5-2843-2012>.
- Bleck R. , Rooth C. , Hu D. , Smith L. T . Salinity-driven thermocline transients in a wind- and thermohaline-forced isopycnic coordinate model of the North Atlantic. *J. Phys. Oceanogr.* 1992; 22: 1486–1505.
- Craig A. P., Vertenstein M., Jacob R. A new flexible coupler for earth system modeling developed for CCSM4 and CESM1. *Int. J. High Perform. Comput. Appl.* 2011; 26: 31–42. DOI: <http://dx.doi.org/1094342011428141>.
- Christian, J. R. and R. Murtugudde, 2003: Tropical atlantic variability in a coupled physical–biogeochemical ocean model. *Deep Sea Research Part II: Topical Studies in Oceanography*, 50 (22), 2947–2969.
- Deppenmeier, Haarsma and Hazeleger, 2017: “Ocean mixing – SST – cloud cover – shortwave radiation coupling in the tropical Atlantic”. Submitted to *Climate Dynamics*.
- Exarchou, E., C. Prodhomme, L. Brodeau, F. Doblas-Reyes, 2016: Origin of the warm eastern tropical Atlantic SST bias in a climate model. *Climate Dynamics*, under review.
- Ferry, N., et al., 2010. Mercator Global Eddy Permitting Ocean Reanalysis GLORYS1V1: Description and Results. *Mercator Ocean Quarterly Newsletter*, 36. p. 15-27.
- Goubanova K, E. Sanchez Gomez, C. Frauen and A. Voltaire: Role of the remote and local wind stress forcing in the development of the warm SST errors in the South-Eastern Tropical Atlantic in a coupled high-resolution seasonal hindcast, to be submitted to *Climate Dynamics*
- Jouanno, J., F. Marin, Y. du Penhoat, J. Sheinbaum, and J. M. Molines, 2011: Seasonal heat balance in the upper 100 m of the equatorial Atlantic Ocean. *J. Geophys. Res.*, 116, C09003, doi:10.1029/2010JC006912
- Kirkevåg A. , Iversen T. , Seland Ø. , Hoose C. , Kristjánsson J. , co-authors . Aerosol–climate interactions in the Norwegian Earth System Model–NorESM1-M. *Geosci. Model Dev.* 2013; 6(1): 207–244.
- Lengaigne, M., C. Menkes, O. Aumont, T. Gorgues, L. Bopp, J.-M. André, and G. Madec, 2007: Influence of the oceanic biology on the tropical pacific climate in a coupled general circulation model. *Climate Dynamics*, 28 (5), 503–516.
- Neale R. B. , Chen C.-C. , Gettelman A. , Lauritzen P. H. , Park S. , co-authors . Description of the NCAR Community Atmosphere model (CAM 4.0). 2010. NCAR Tech. Note NCAR/TN-486+ STR.
- Monerie, PA., Coquart, L., Maisonnave, E. et al. MP Moine, L. Terray, S. Valcke (2017) Decadal prediction skill using a high-resolution climate model, *Clim Dyn*, doi:10.1007/s00382-017-3528-x.
- Monger, B., C. McClain, and R. Murtugudde, 1997: Seasonal phytoplankton dynamics in the eastern tropical atlantic. *Journal of Geophysical Research: Oceans*, 102 (C6), 12 389–12 411.

Peter, C., M. L. Hénaff, Y. du Penhoat, C. Menkès, F. Marin, J. Vialard, G. Caniaux, and A. Lazar (2006), A model study of the seasonal mixed-layer heat budget in the equatorial Atlantic. *J. Geophys. Res.*, 111, C06014, doi:10.1029/2005JC003157.

Pillar, H, Jochum, M., Nuterman, R., Bensten, M., and T. Toniazzo (2017): «Dominance of tropical wind-generated inertial current in setting the global response to upper ocean inertial mixing. To be submitted to *J. Climate*.

Richter, I. and S. P. Xie, 2008: On the origin of equatorial Atlantic biases in coupled general circulation models. *Climate Dynamics*, 31 (5), 587–598, doi:10.1007/s00382-008-0364-z.

Richter, I., 2015: Climate model biases in the eastern tropical oceans: causes, impacts and ways forward. *Wiley Interdisciplinary Reviews: Climate Change*, 6 (3), 345–358, doi:10.1002/wcc.338, URL <http://doi.wiley.com/10.1002/wcc.338>.

Shonk, J.P.S., Guyliardi, E., Toniazzo, T., Woolnough, S.J., and T. Stockdale (2017): Identifying causes of Western Pacific ITCZ drift in ECMWF System 4 hindcasts. *Clim. Dyn.* DOI 10.1007/s00382-017-3650-9

Siongco A. C., Hoheneger, C. and Stevens B., 2017, Sensitivity of the summertime tropical Atlantic precipitation distribution to convective parameterization and model resolution in ECHAM6, *J. of Geophys. Res. A.*: 2579-2594, doi: 10.1002/2016JD026093.

Tjiputra J. , Roelandt C. , Bentsen M. , Lawrence D. , Lorentzen T. , co-authors, 2013: Evaluation of the carbon cycle components in the Norwegian Earth System Model (NorESM). *Geosci. Model Dev*, 6(2): 301–325.

Toniazzo, T. and S. Woolnough, 2013: Development of warm SST errors in the southern tropical Atlantic in CMIP5 decadal hindcasts. *Climate Dynamics*, doi:10.1007/s00382-013-1691-2, URL <http://link.springer.com/10.1007/s00382-013-1691-2>.

Vertenstein M., Craig T., Middleton A., Feddema D., Fischer C. CESM1.0.3 user guide. 2012. Online at: [http://www.cesm.ucar.edu/models/cesm1.0/cesmcesm\\_doc\\_1\\_0\\_3ug.pdf](http://www.cesm.ucar.edu/models/cesm1.0/cesmcesm_doc_1_0_3ug.pdf).

Voldoire, A., E. Sanchez-Gomez, D. Salas y Méliá, B. Decharme, C. Cassou, S. Sénési, S. Valcke, I. Beau, A. Alias, M. Chevallier, M. Déqué, J. Deshayes, H. Douville, E. Fernandez, G. Madec, E. Maisonnave, M.-P. Moine, S. Planton, D. Saint-Martin, S. Szopa, S. Tyteca, R. Alkama, S. Belamari, A. Braun, L. Coquart, F. Chauvin., 2013: The CNRM-CM5.1 global climate model: description and basic evaluation. *Clim. Dyn.*, 40(9-10):2091-2121, doi:10.1007/s00382-011-1259-y.

**FIGURES**

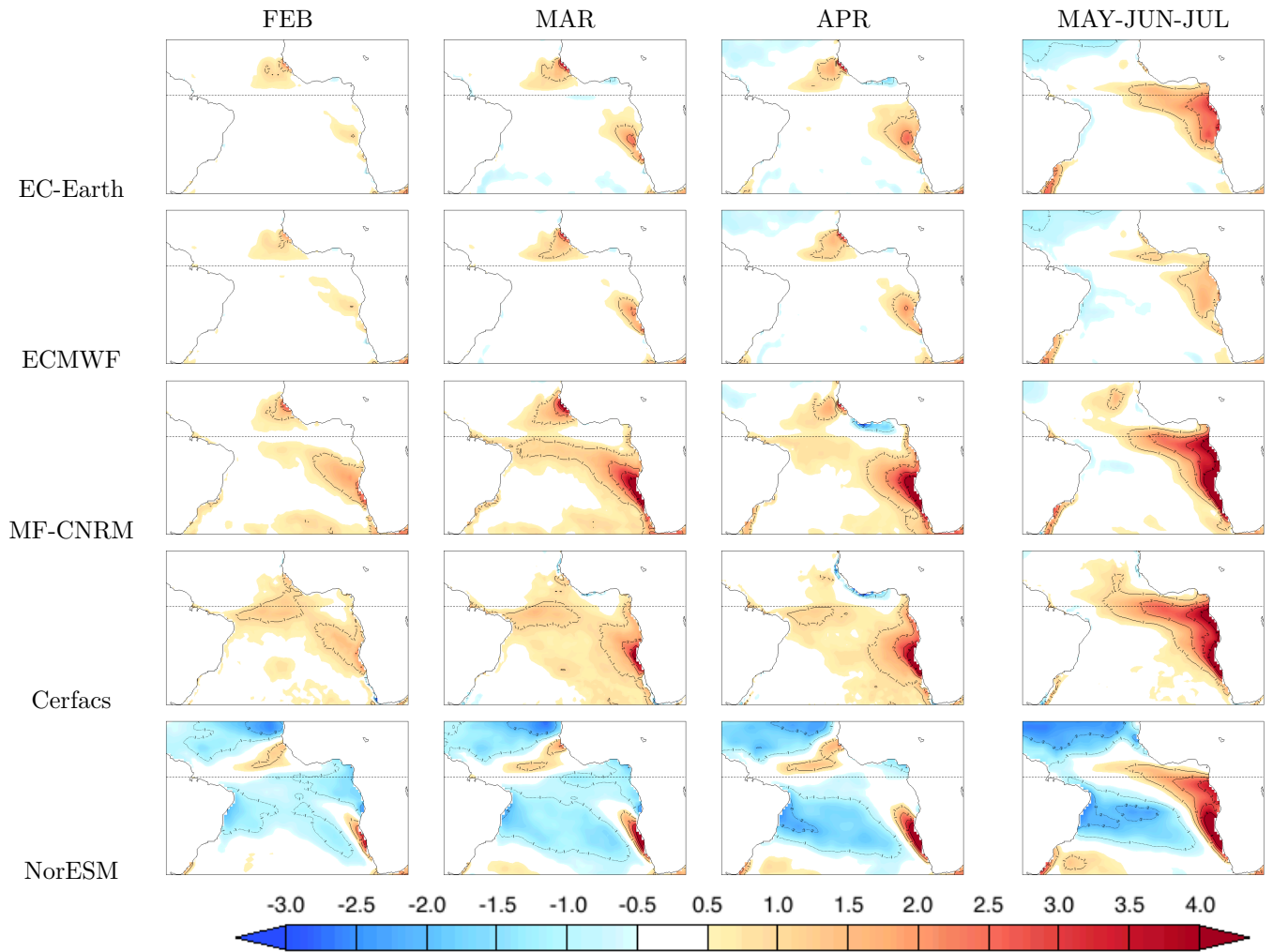


Figure 1: SST error (K) to the HadISST data for one-month lead-time (first column), 2 months (second column), 3 months (3rd column) and averaged over lead-time 3-5 months (4th column) for the EC-Earth model (top row), ECMWF model (2nd row), MF-CNRM model (3rd row), Cerfacs (4th row) and NorESM (5th row) for February starts.

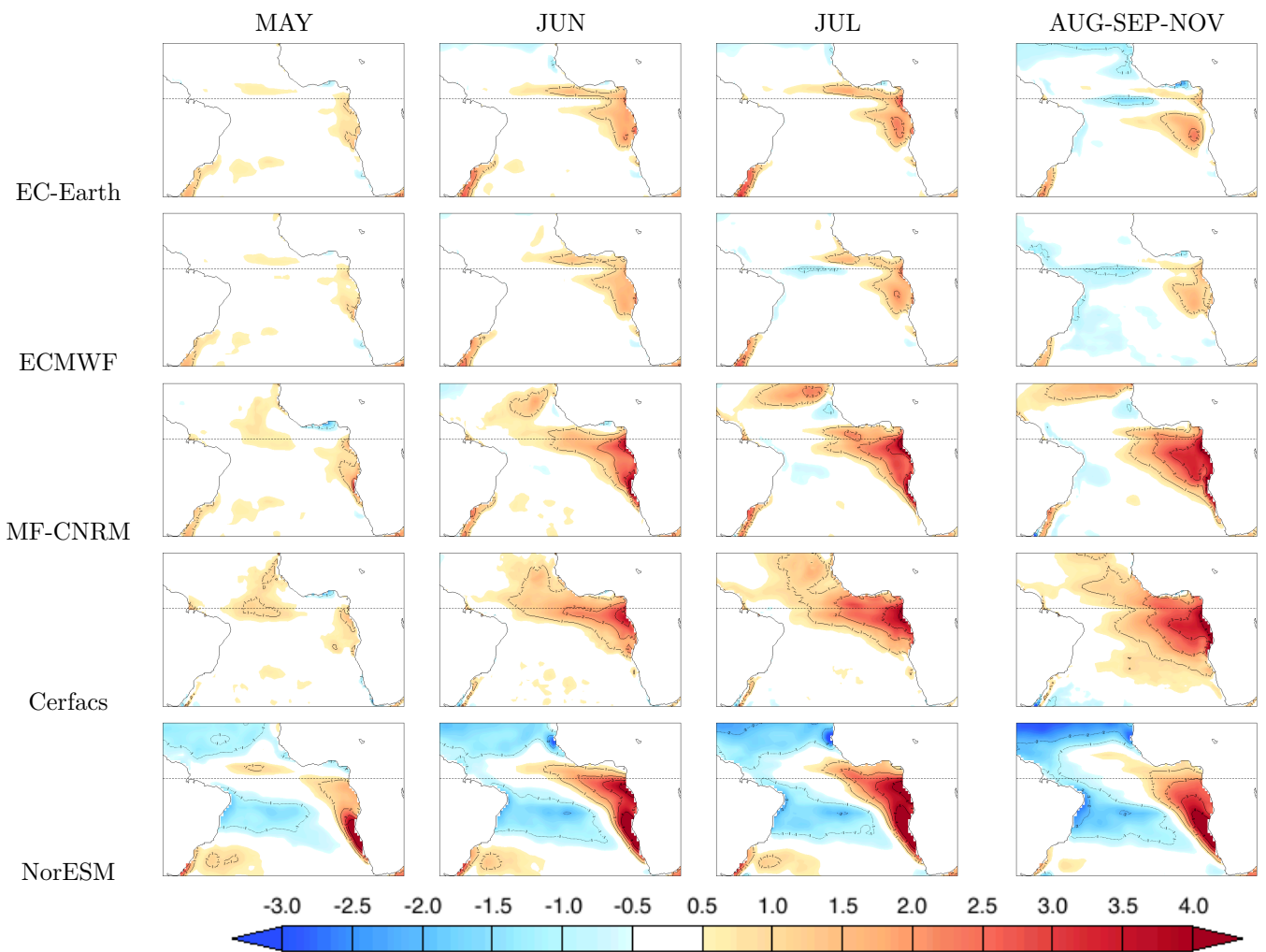


Figure 2: Same as fig 1 for May starts

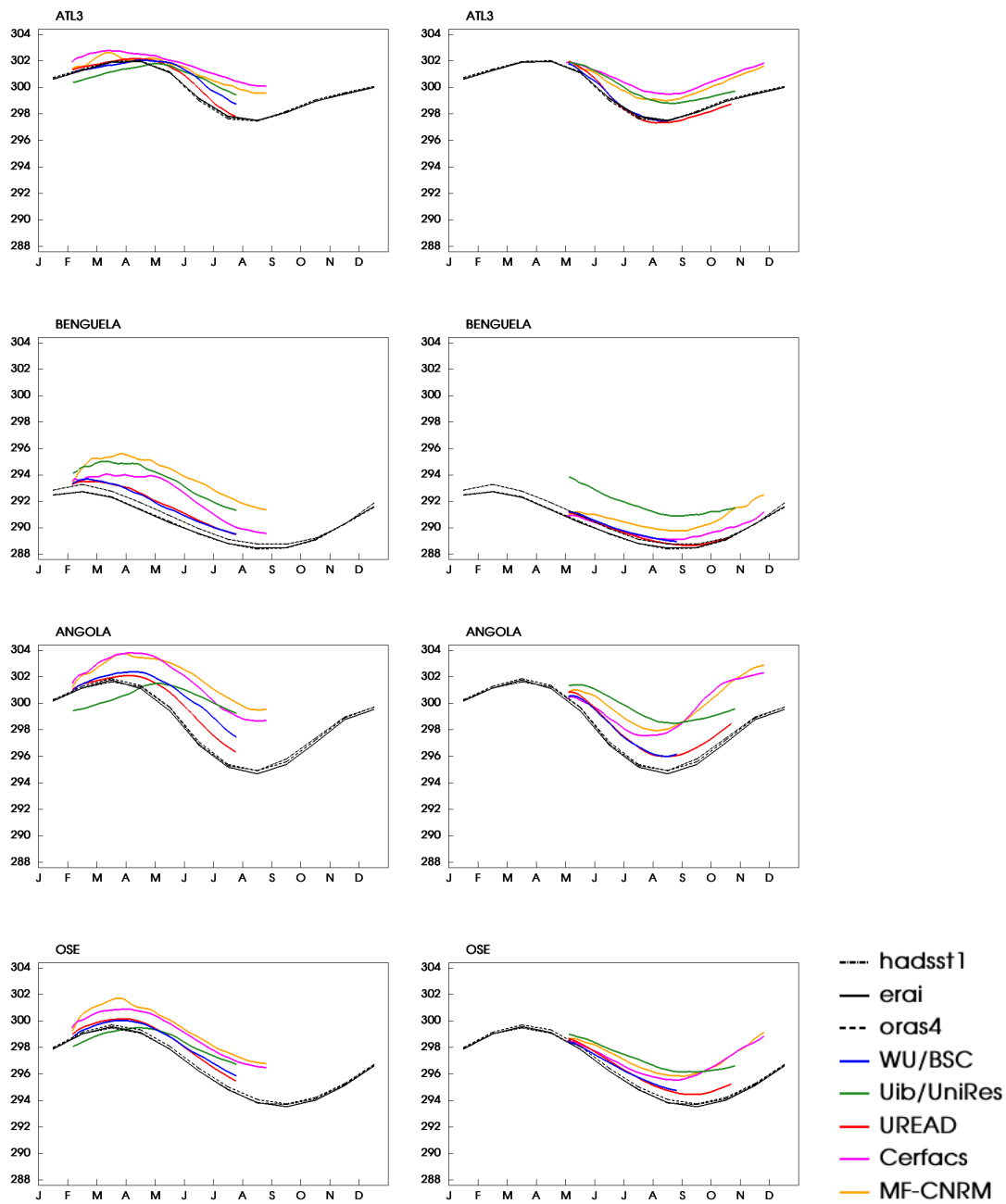


Figure 3: Daily SST evolution (in K) in CTRL (color lines, see legend), for February starts (left) and May starts (right) over ATL3 [3S-3N, 20W-0E] (first row), BENGUELA [32S-20S, 12E-Coast] (second row), ANGOLA [15S-3S, 10E-Coast] (third row), OSE [20S-5S, 0-10E] (fourth row); black lines indicate reference monthly mean values for several datasets (reanalysis and observationnaly derived, see legend).

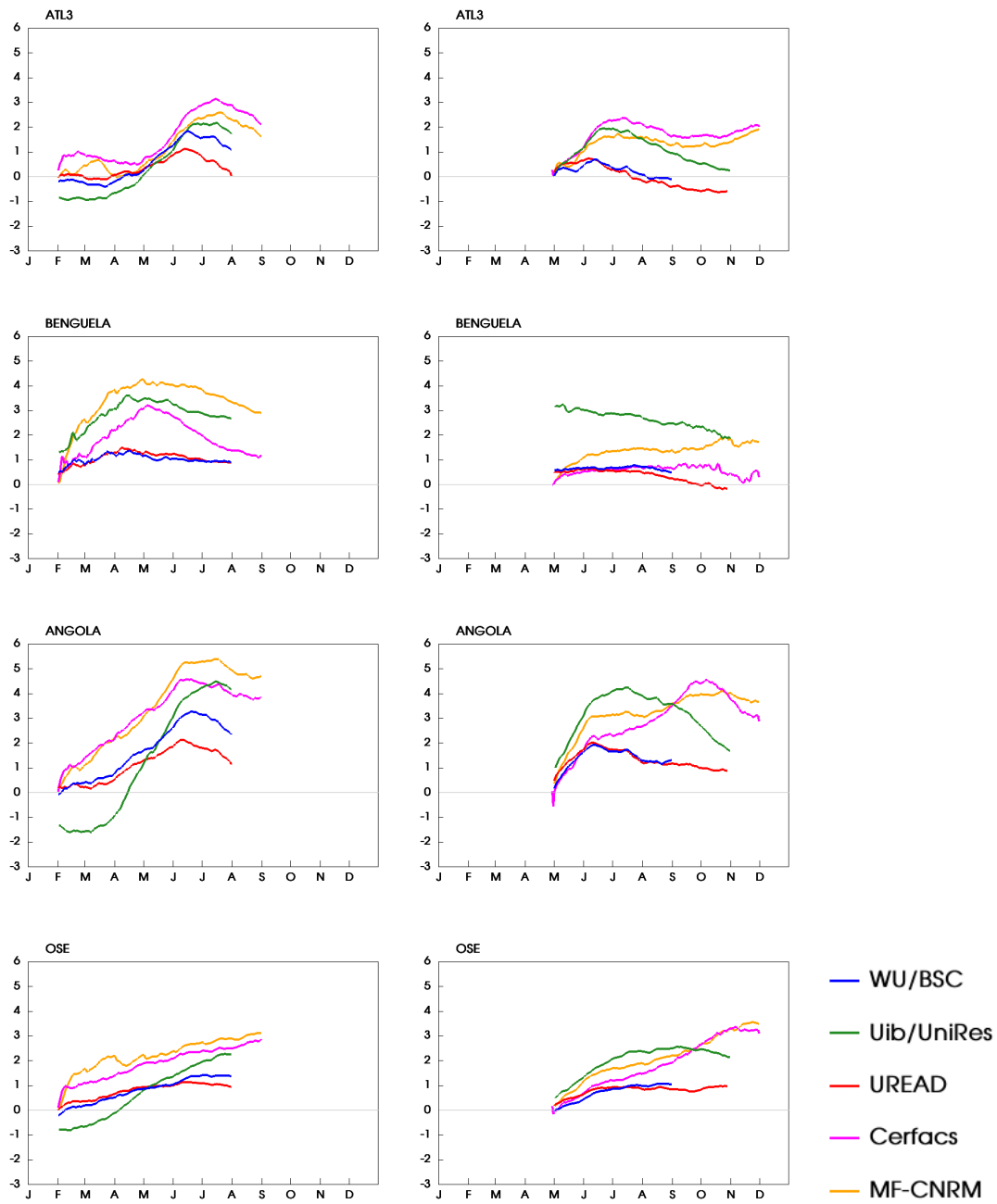


Figure 4: SST error growth (in K) in CTRL, for February starts (left) and May starts (right).

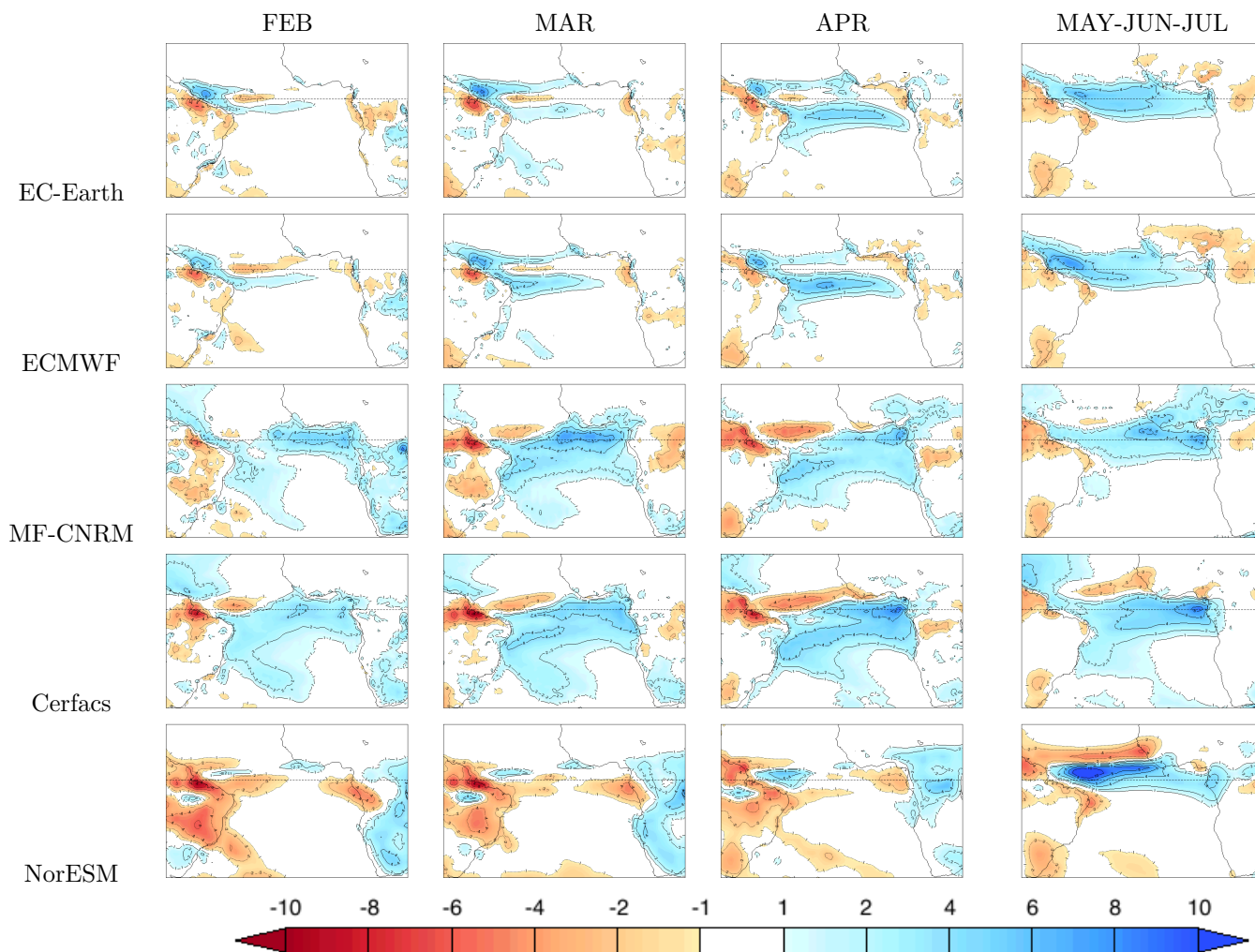


Figure 5: Precipitation error ( $\text{mm.d}^{-1}$ ) to the GPCP data for one-month lead-time (first column), 2 months (second column), 3 months (3rd column) and averaged over lead-time 3-5 months (4th column) for the EC-Earth model (top row), ECMWF model (2nd row), MF-CNRM model (3rd row), Cerfacs (4th row) and NorESM (5th row) for February starts.

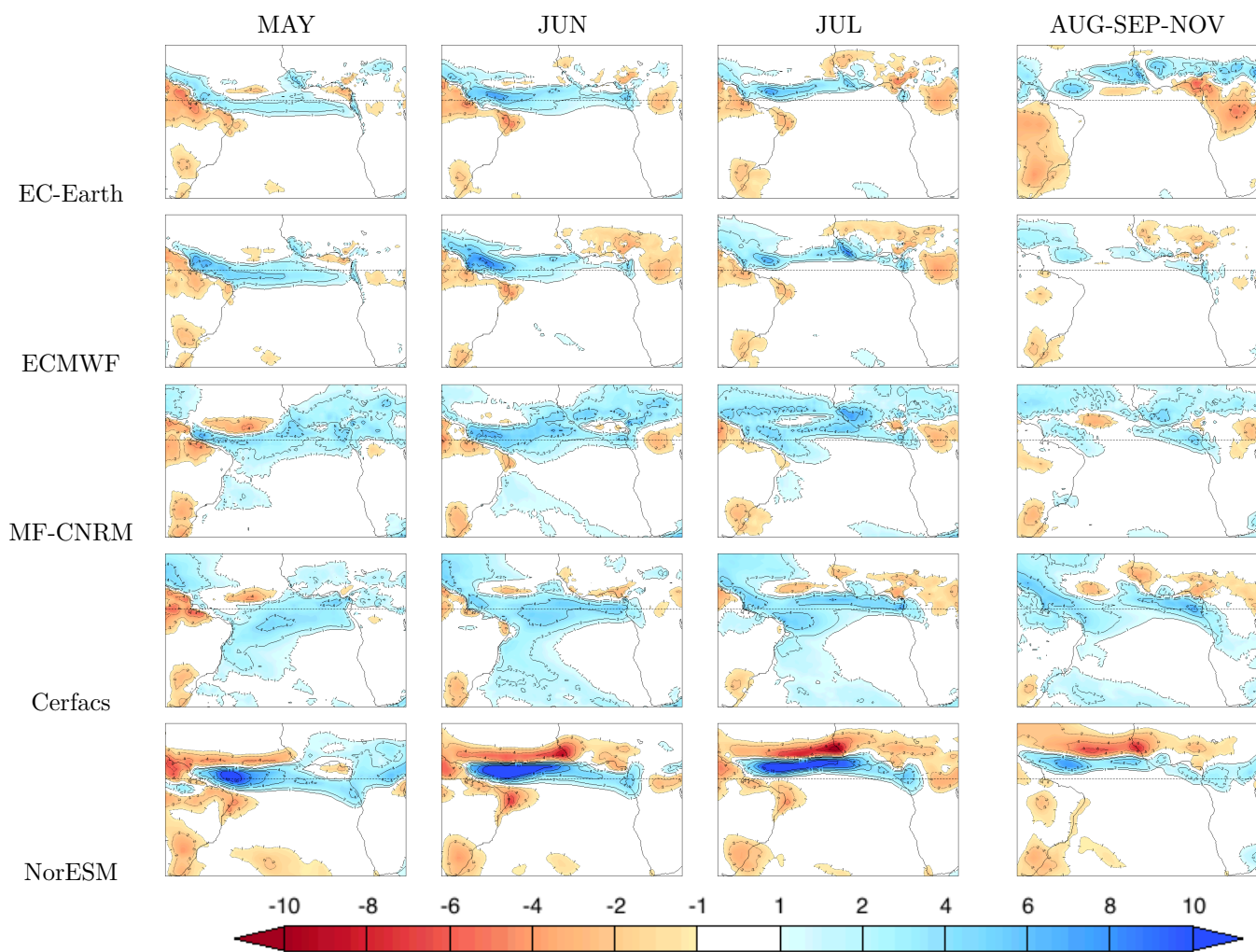


Figure 6: Same as fig 5 for May starts.

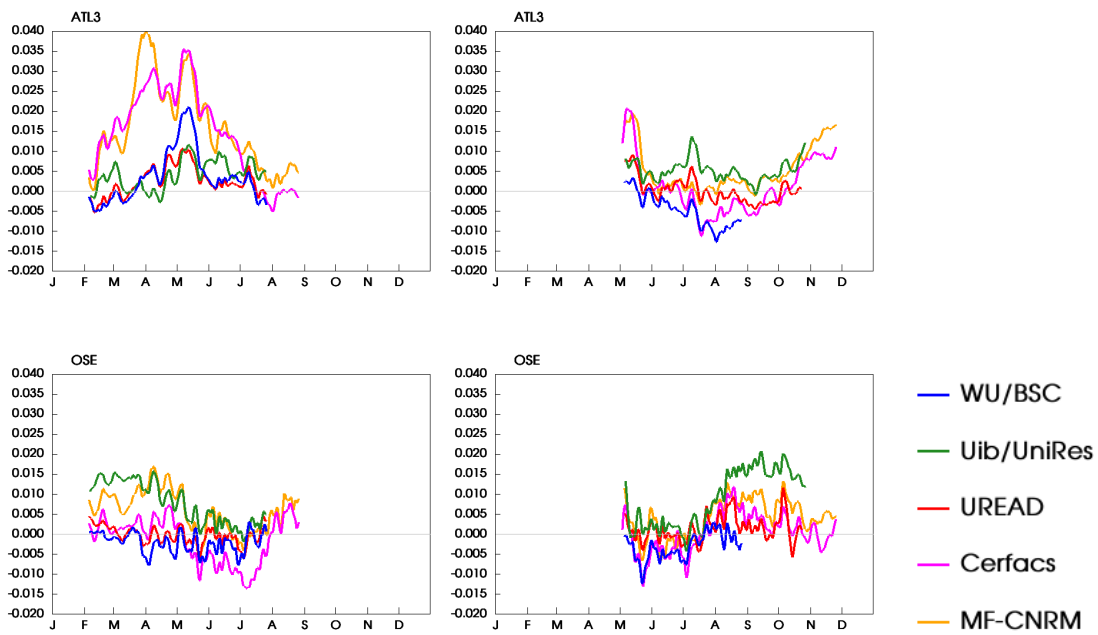


Figure 7: Evolution of the zonal wind stress error ( $\text{N/m}^2$ ) in CTRL, for February starts (left) and May starts (right) over ATL3 (top row) and OSE (bottom row) boxes. Time-series are smoothed using a running mean over 9 days.

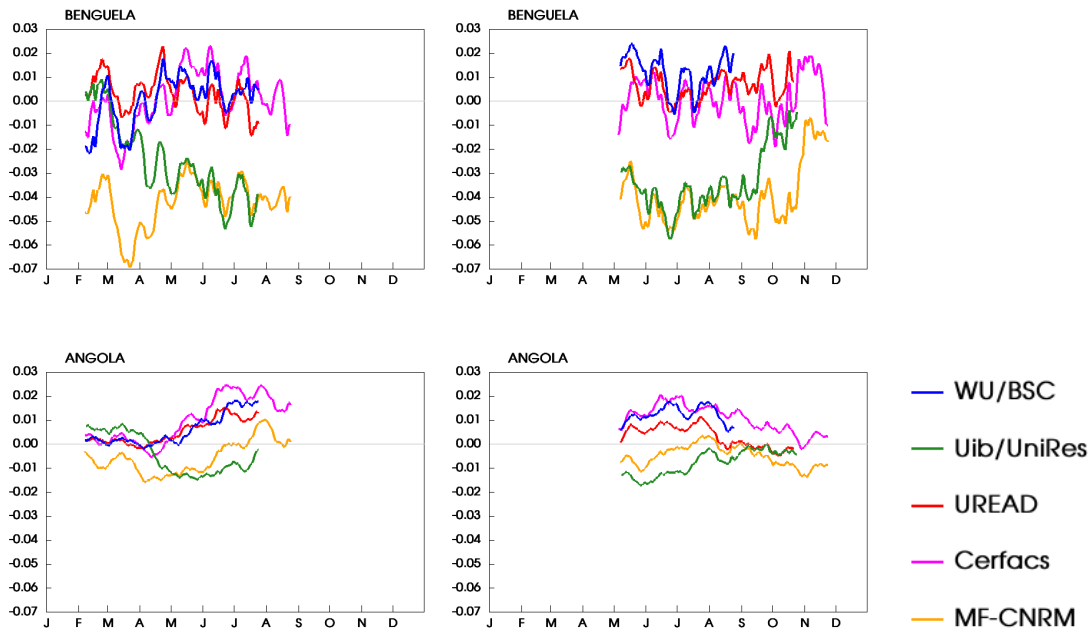


Figure 8: Evolution of the meridional wind stress error ( $N/m^2$ ) in CTRL, for February starts (left) and May starts (right) over BENGUELA (top row) and ANGOLA (bottom row) boxes. Time-series are smoothed using a running mean over 13 days.

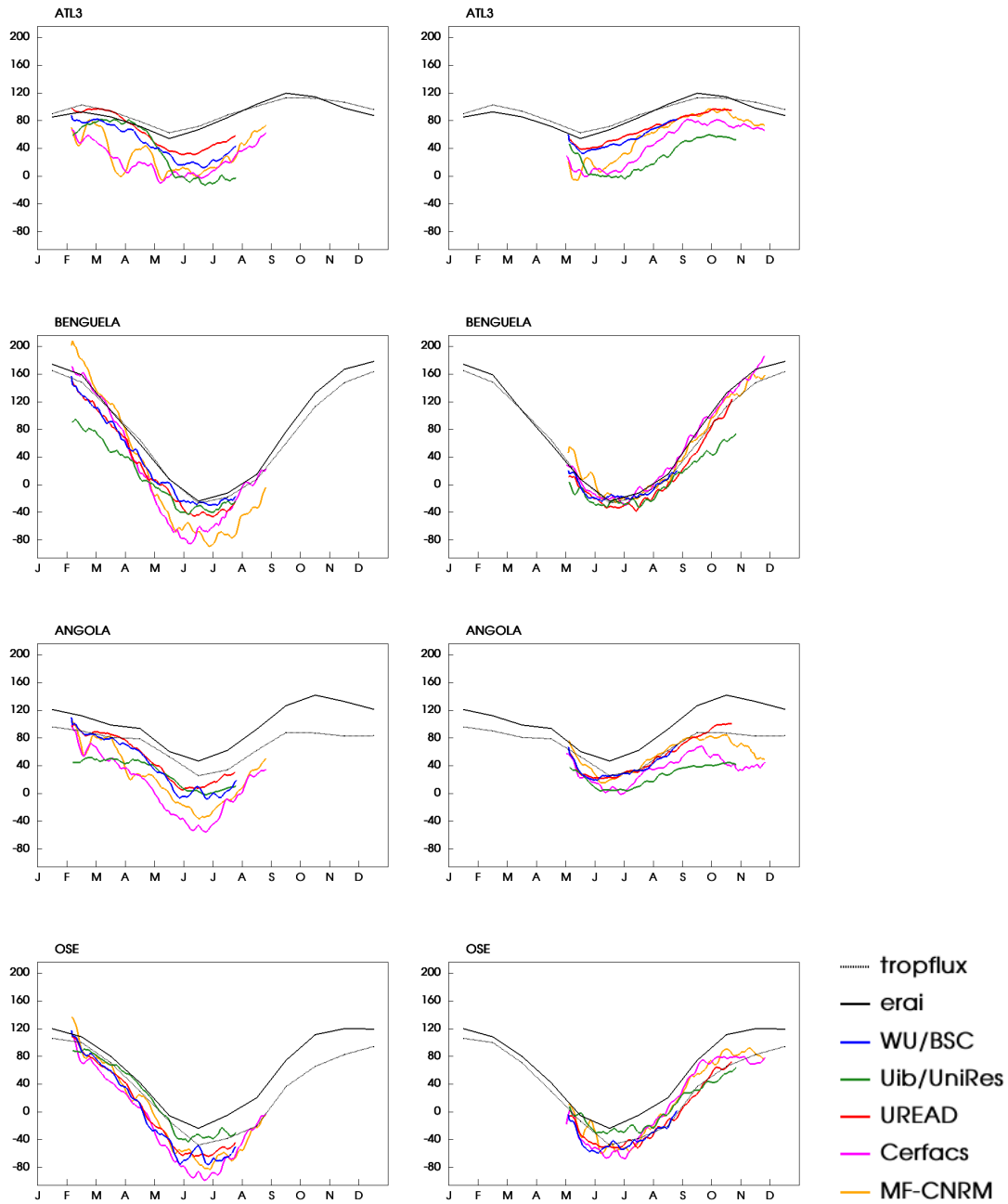


Figure 9: Evolution of the daily net surface heat flux in CTRL ( $\text{W/m}^2$ ) ( $\text{LE}+\text{H}+\text{SW}+\text{LW}$ , color lines), for February starts (left) and May starts (right). Black lines indicate the monthly mean values obtained from era-Interim (solid line) and Tropflux (dashed line).

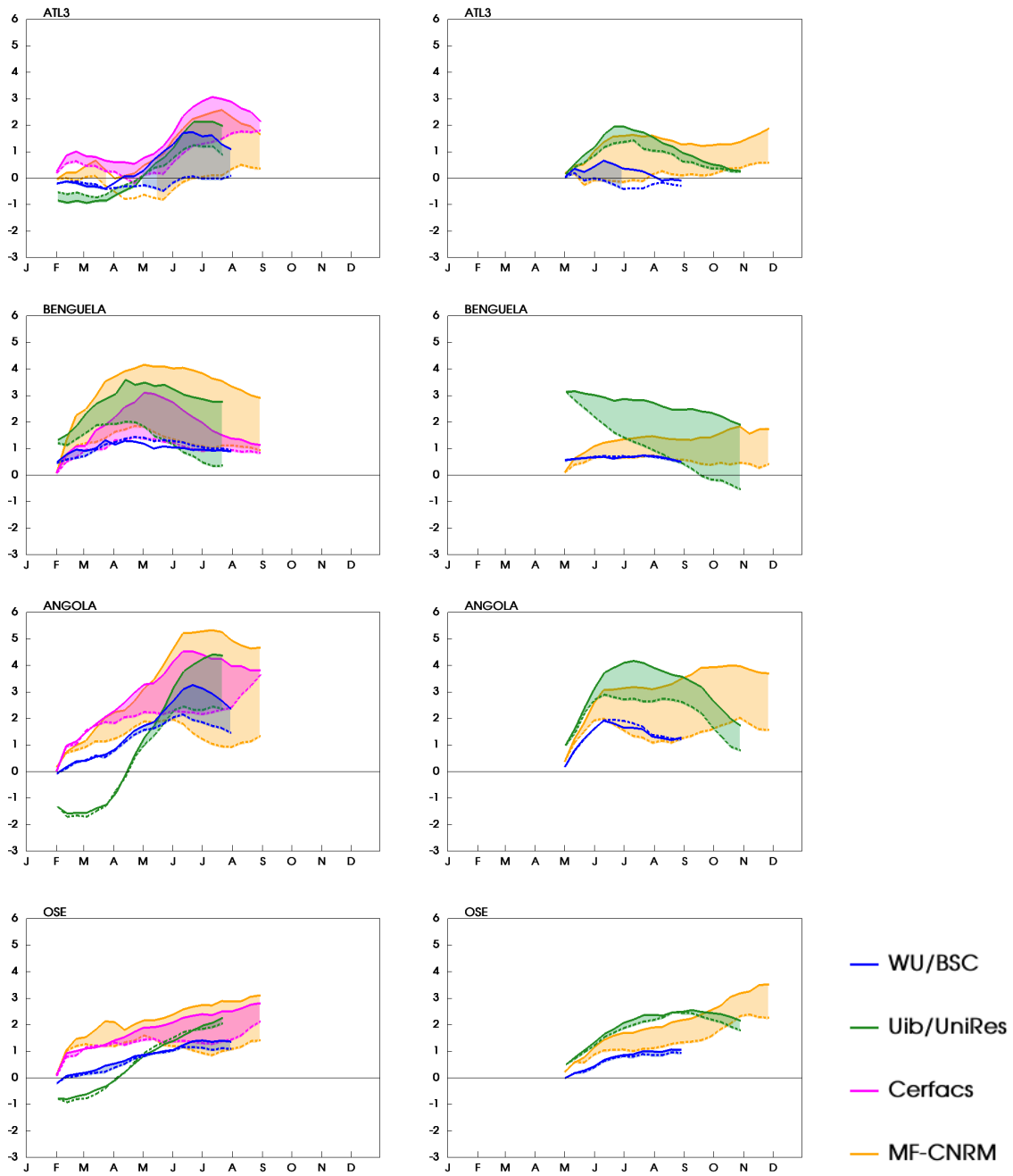


Figure 10: SST error (K) in TAU30 sensitivity experiment (dashed line) versus CTRL experiment (solid line), for February starts (left) and May starts (right). When SST error is reduced in the sensitivity experiment, the difference between the 2 curves is filled.

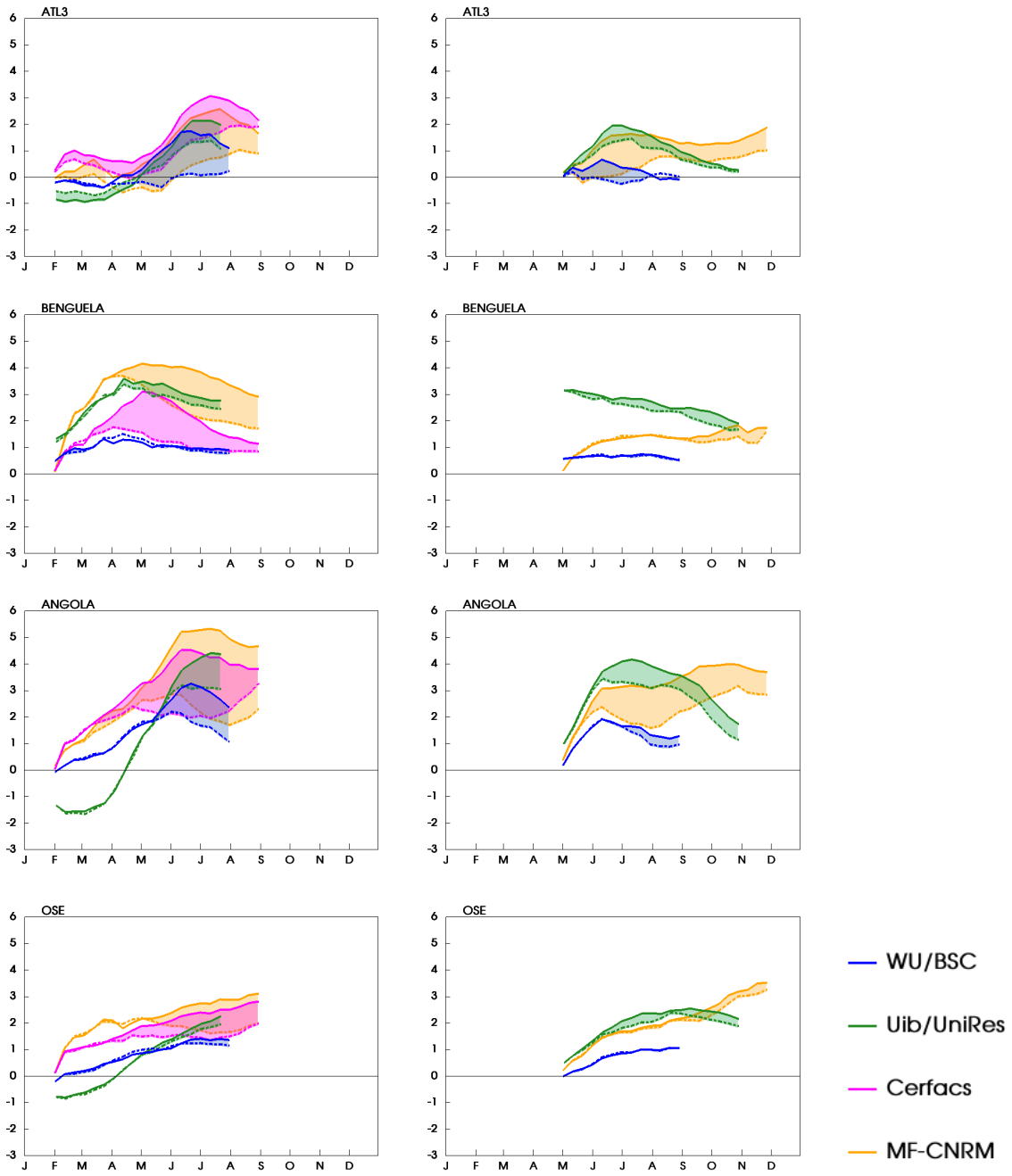


Figure 11: Same as fig 10 for TAUEQ.

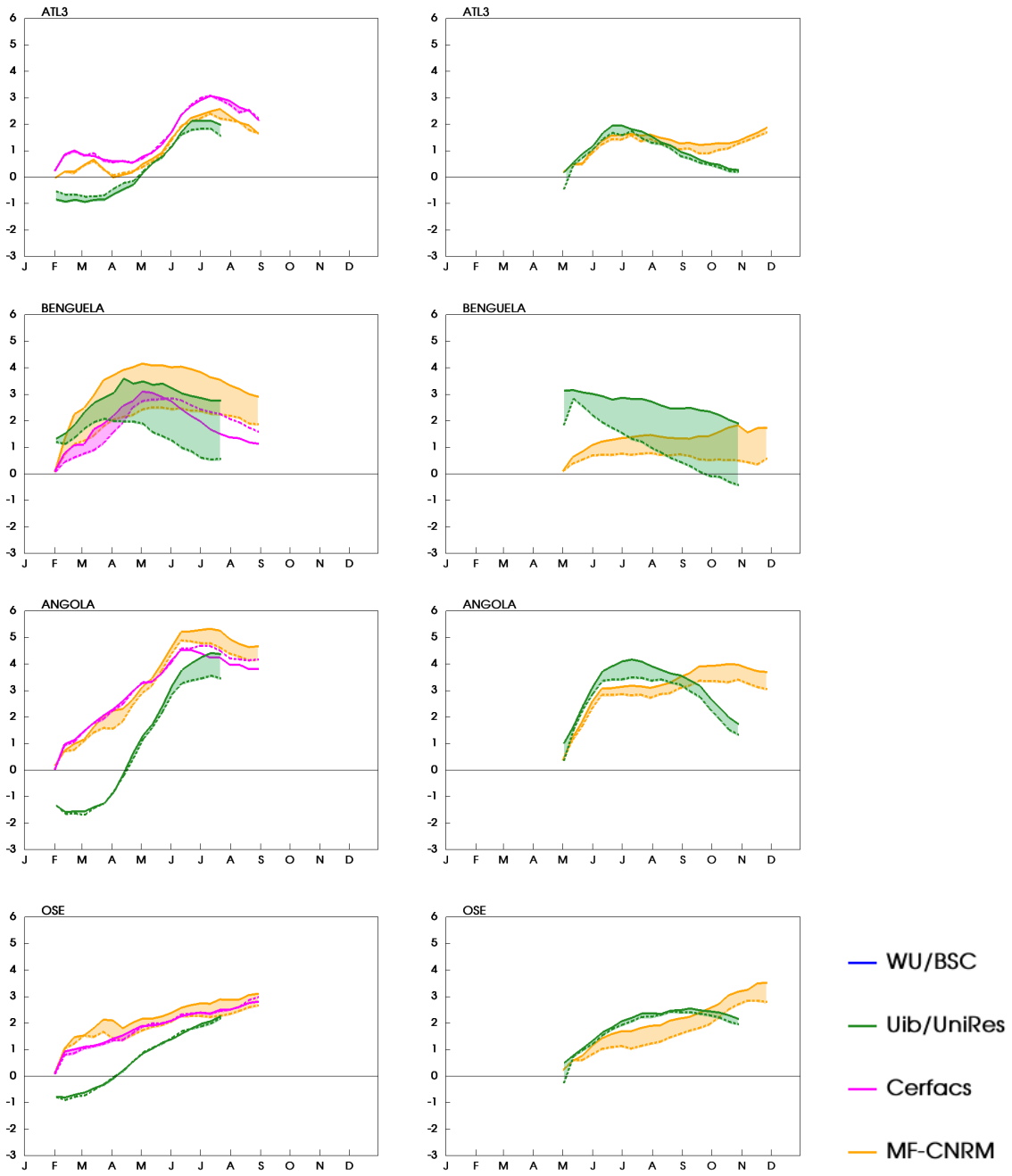


Figure 12: Same as fig 10 for TAUBE.

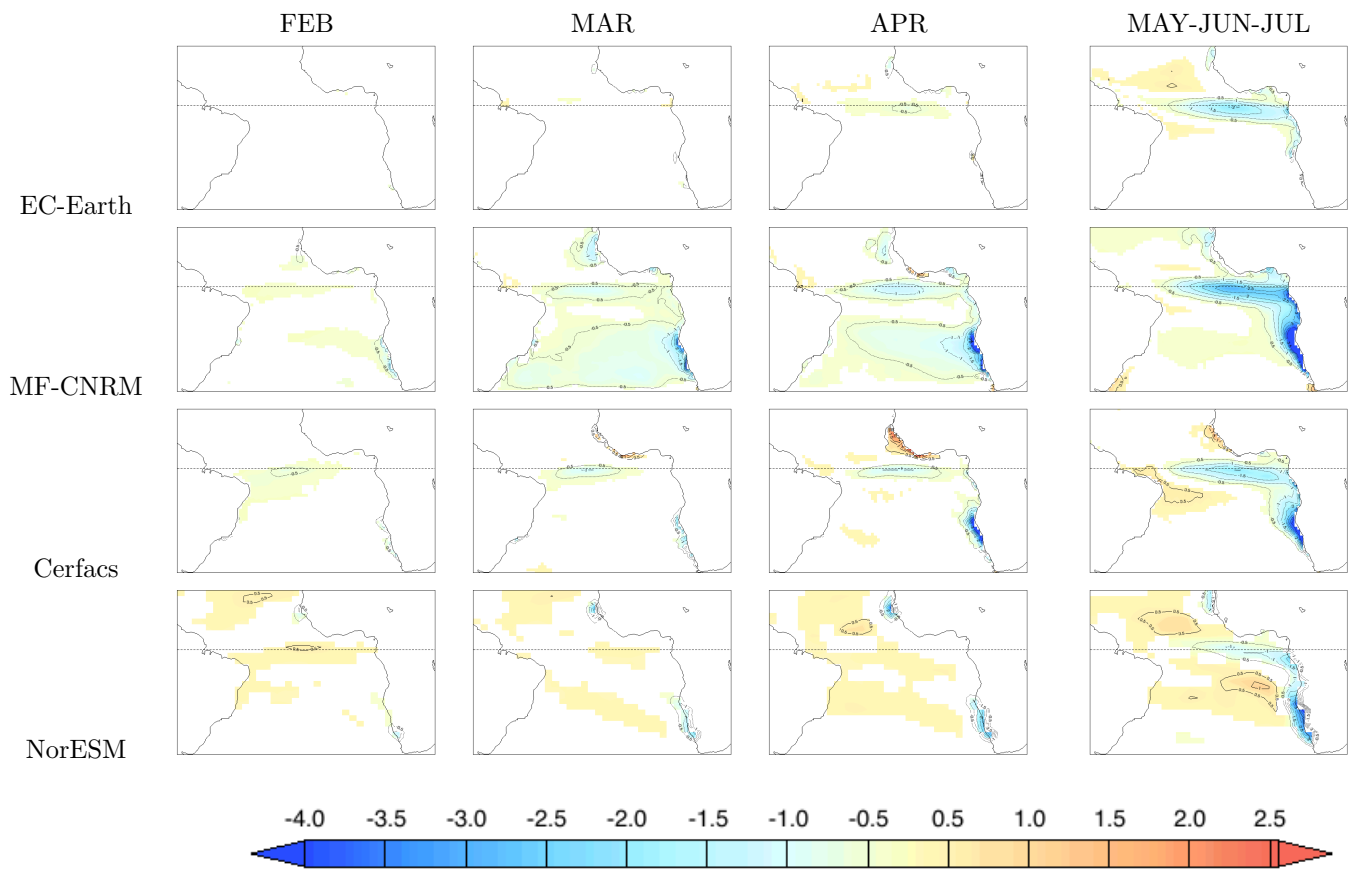


Figure 13: SST (K) difference TAU30-CTRL for February starts

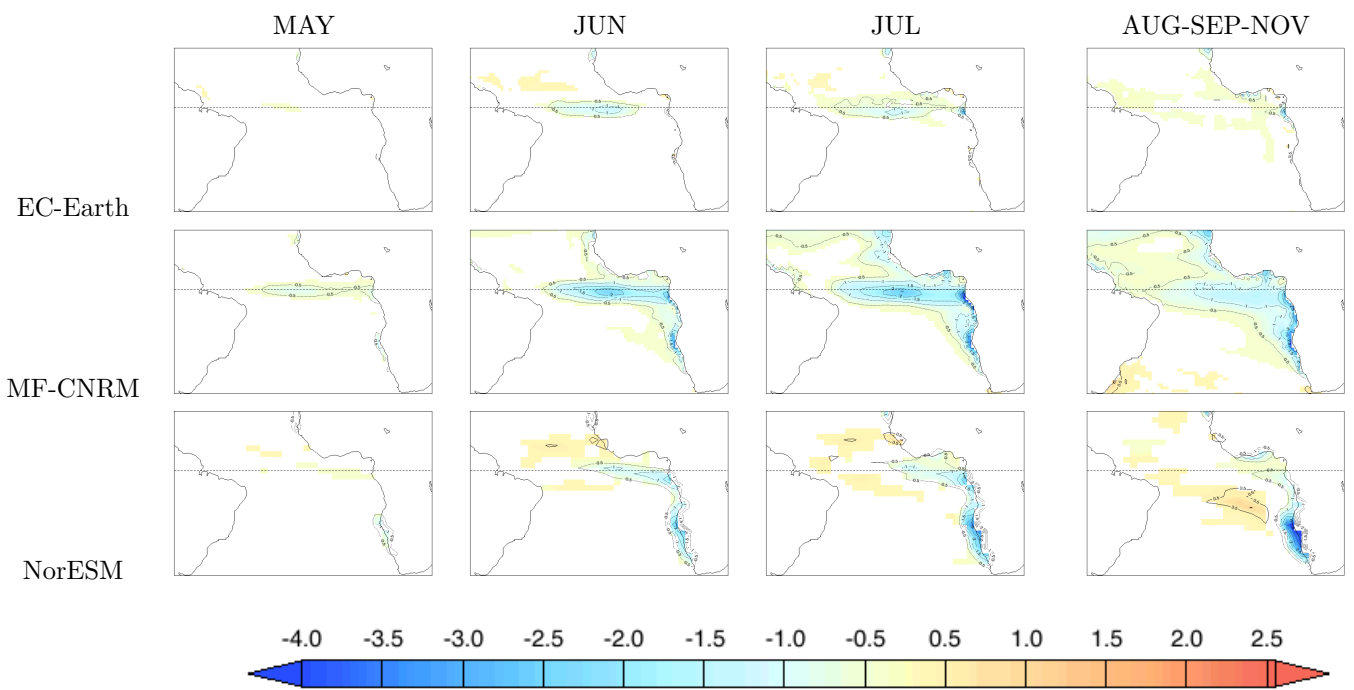


Figure 14: Same as fig 13 for May starts

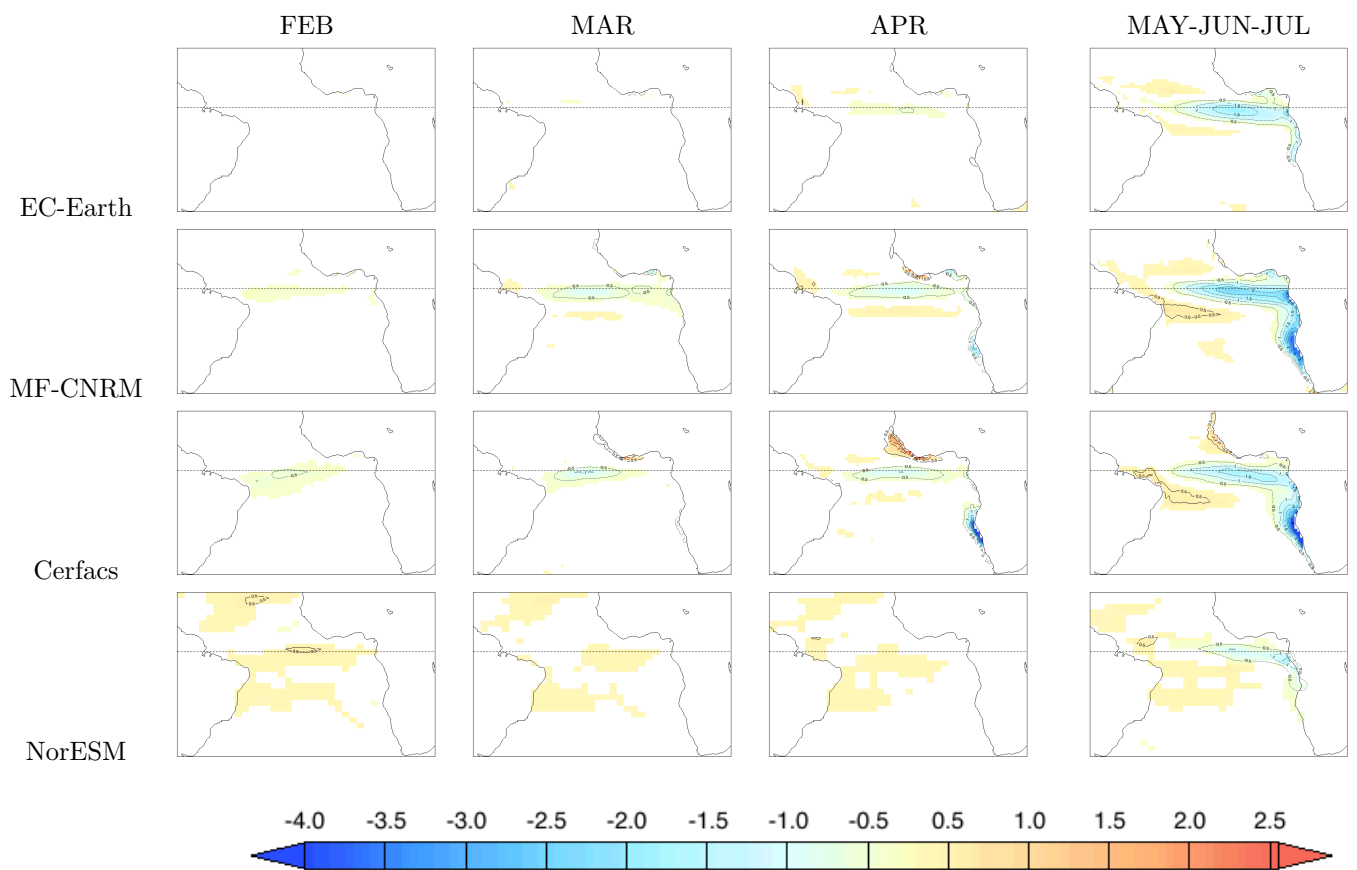


Figure 15: SST (K) difference TAUEQ-CTRL for February starts

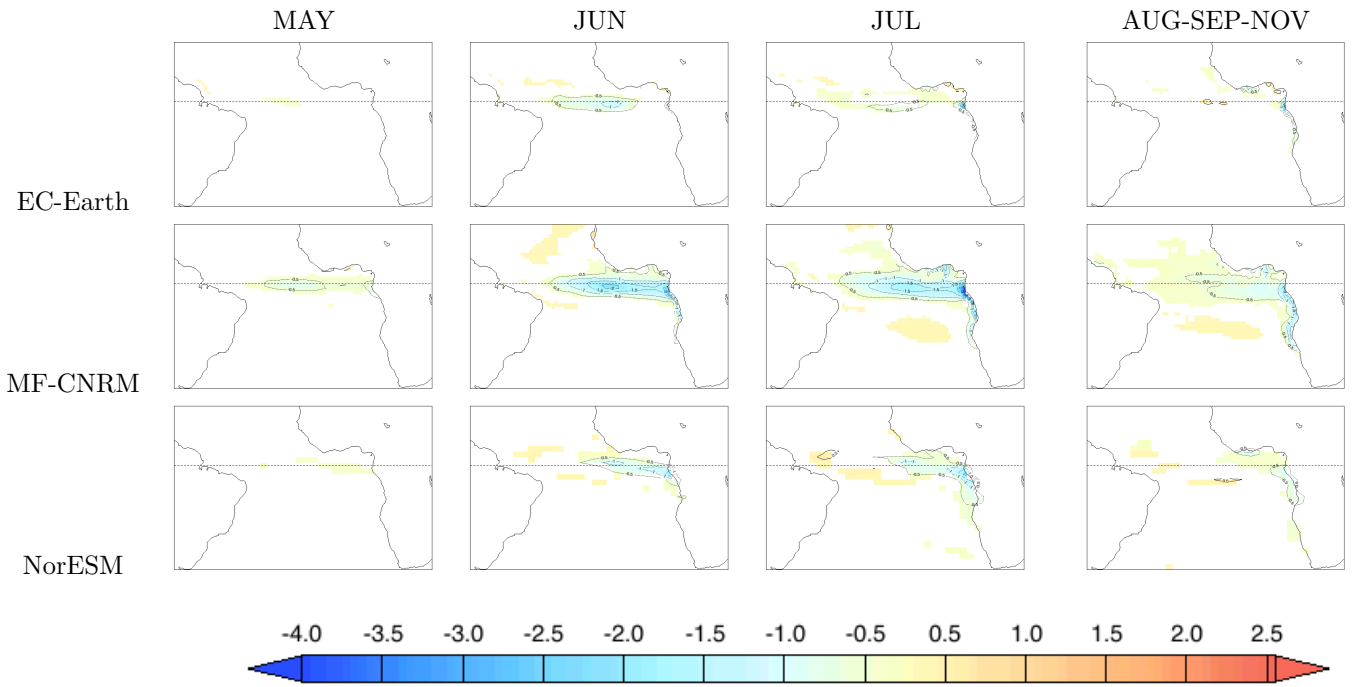


Figure 16: Same as fig 15 for May starts

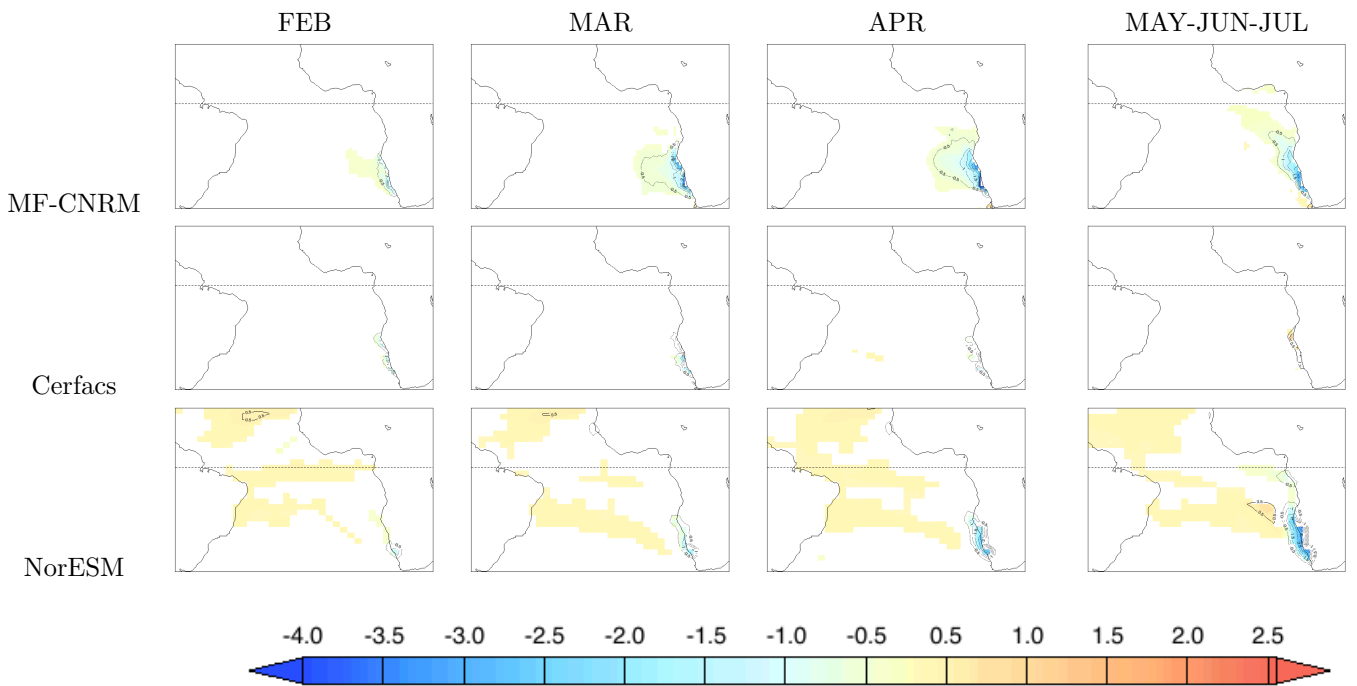


Figure 17: SST (K) difference TAUBE-CTRL for February starts

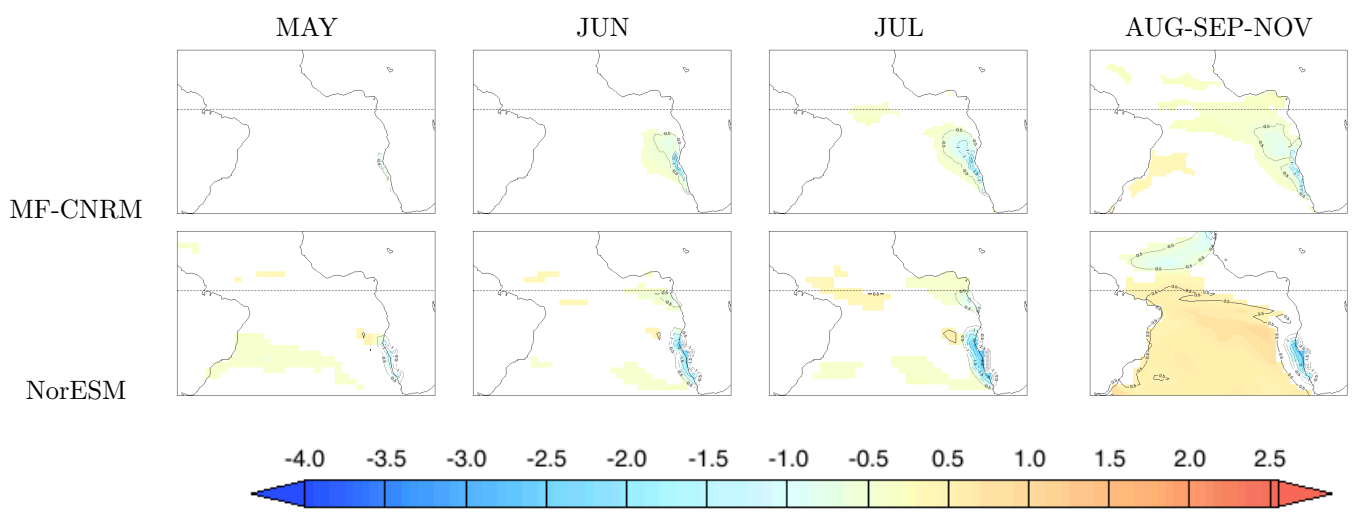


Figure 18: Same as fig 17 for May starts

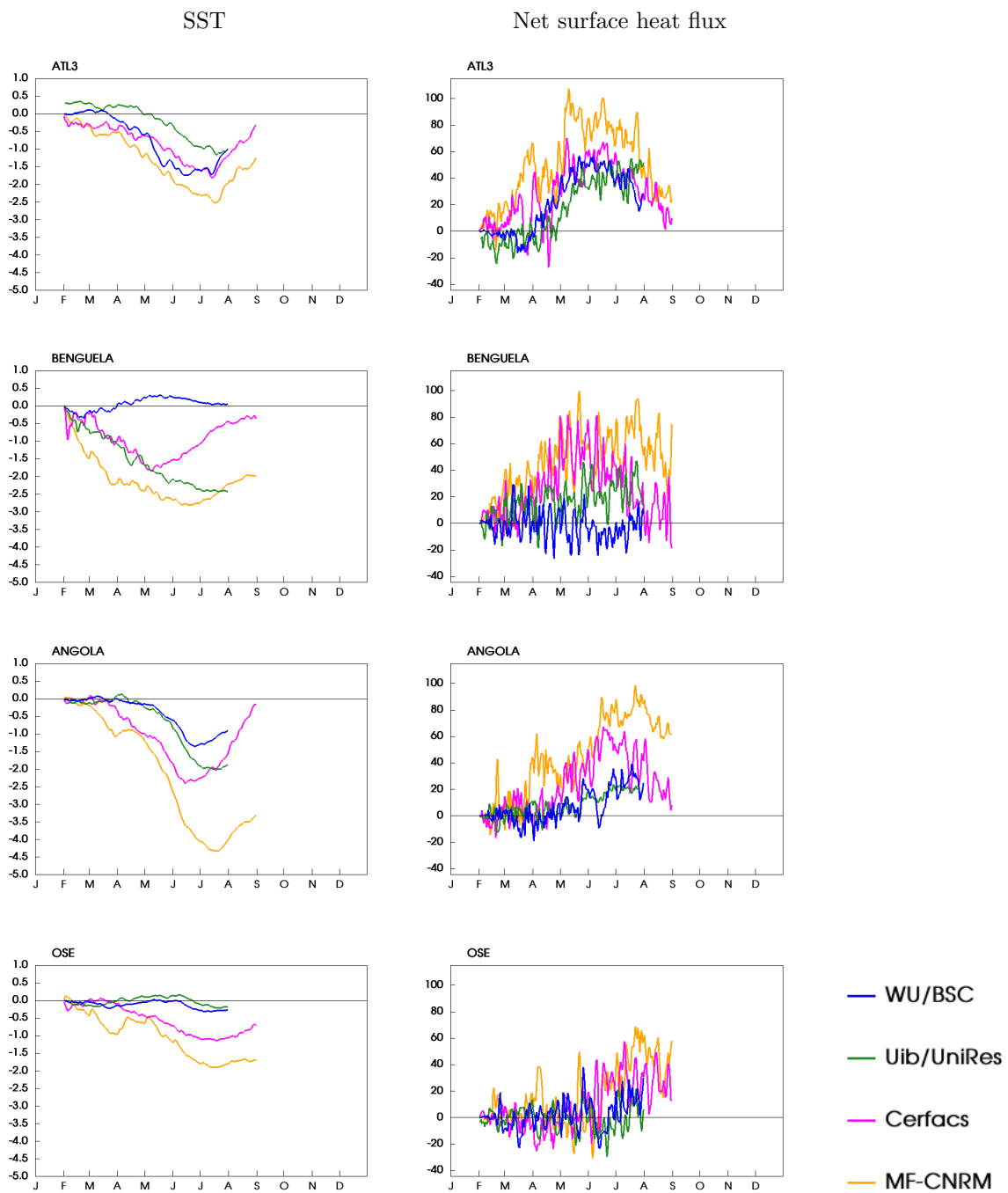


Figure 19: Evolution of the difference between TAU30 and CTRL for SST (left) and net surface heat flux (right) for February starts.

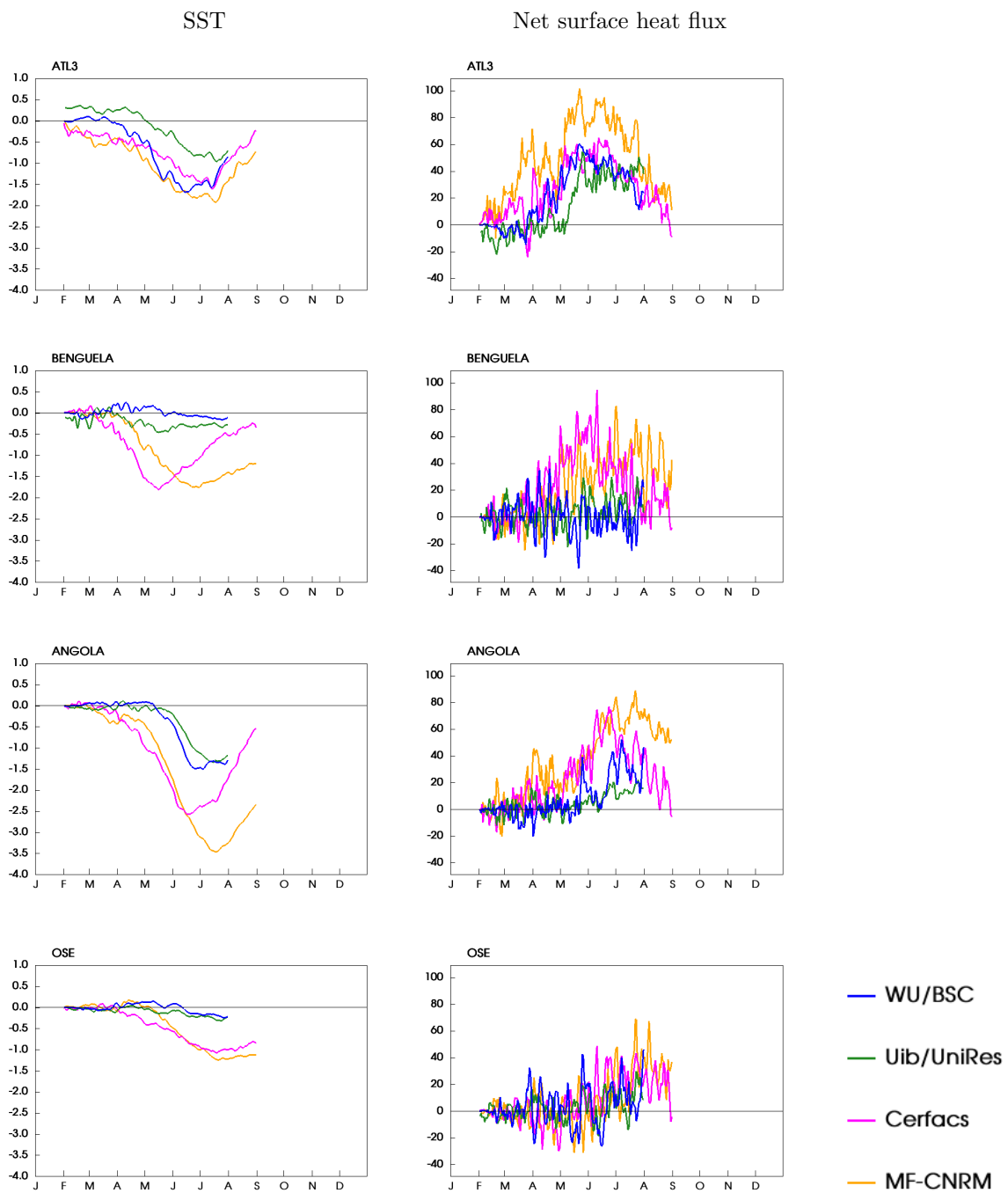


Figure 20: Evolution of the difference between TAUEQ and CTRL for SST (left) and net surface heat flux (right) for February starts.

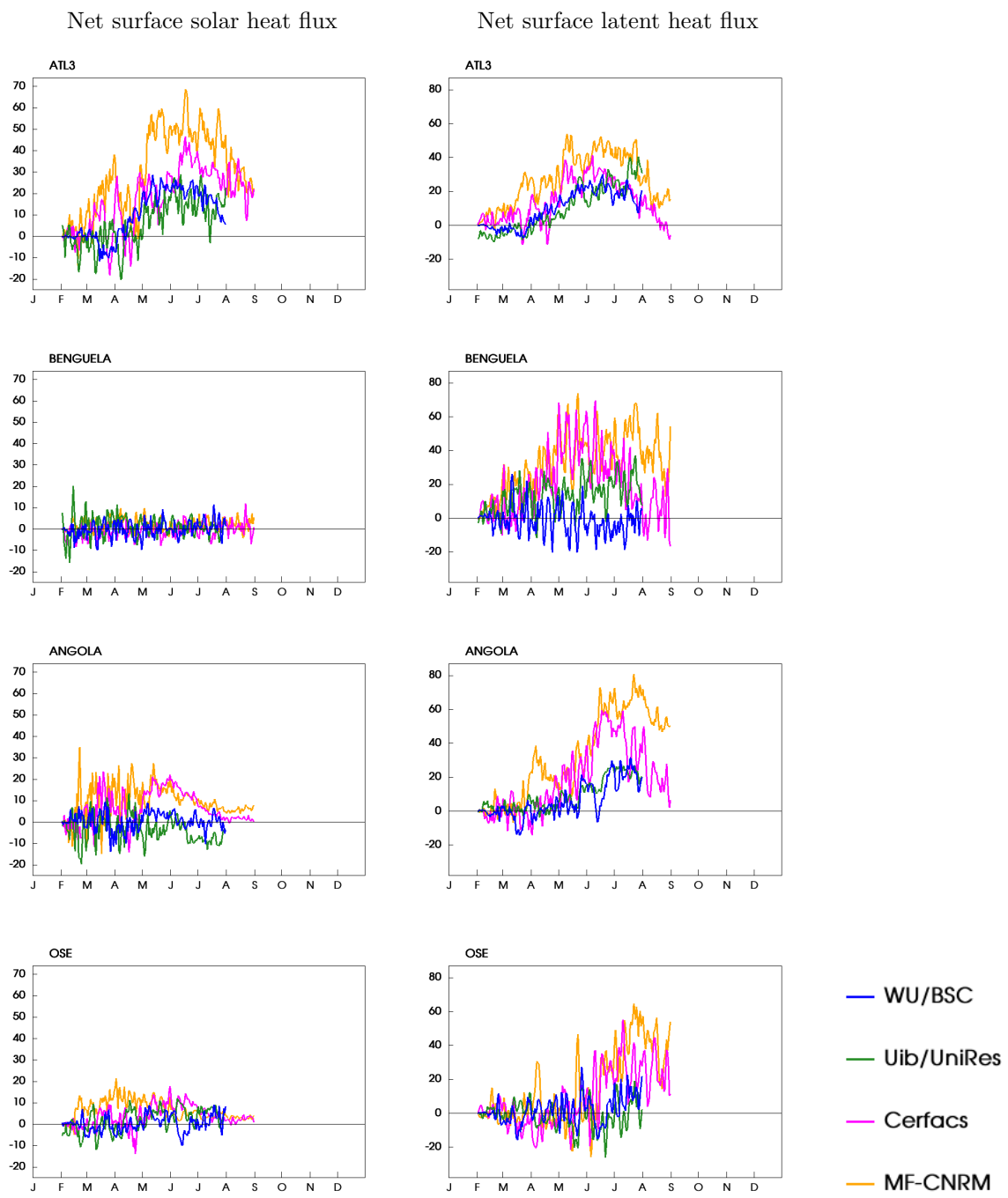


Figure 21: Evolution of the difference between TAU30 and CTRL for net surface solar flux (left) and net surface latent heat flux (right) for February starts.

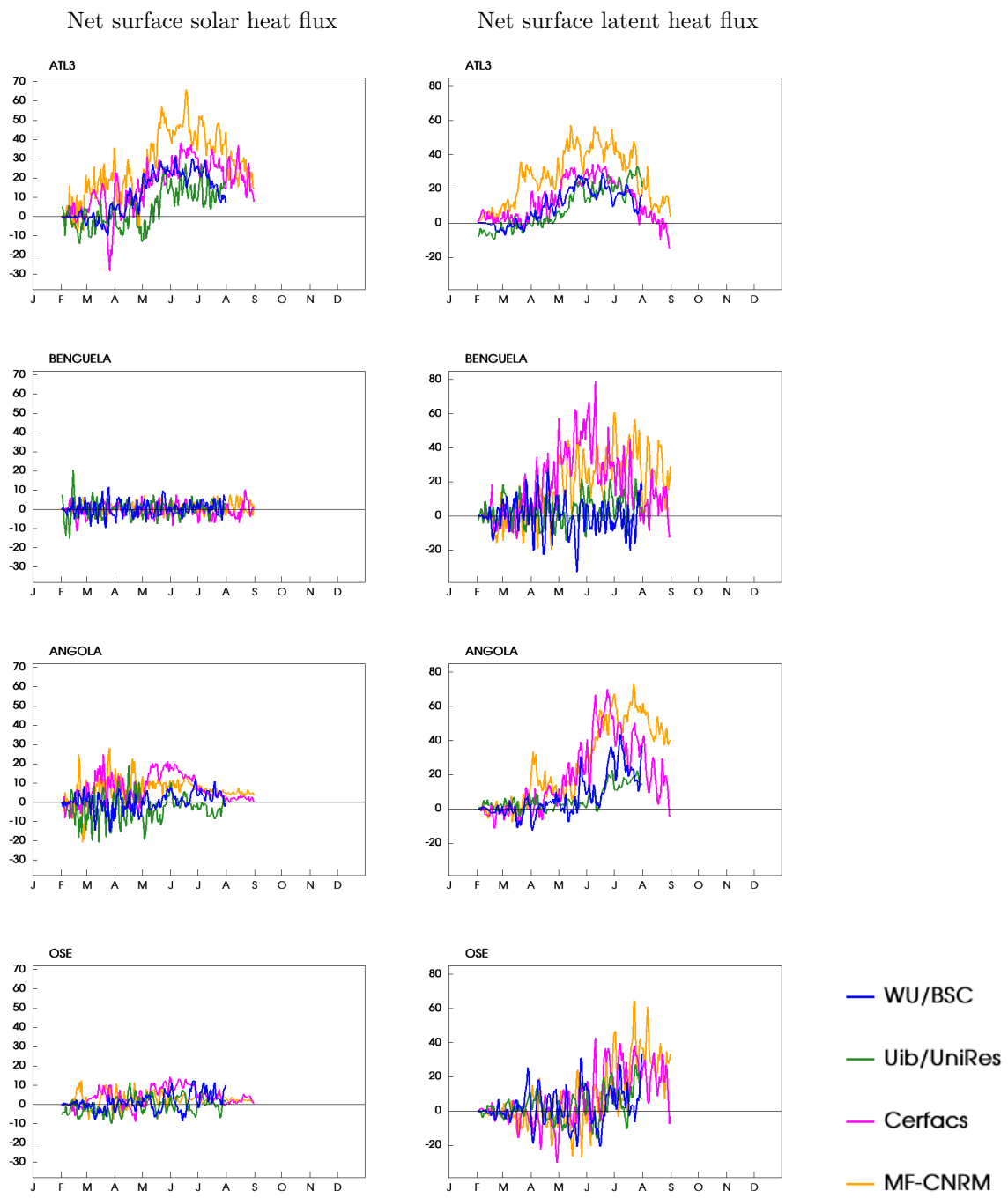


Figure 22: Evolution of the difference between TAUEQ and CTRL for net surface solar flux (left) and net surface latent heat flux (right) for February starts.

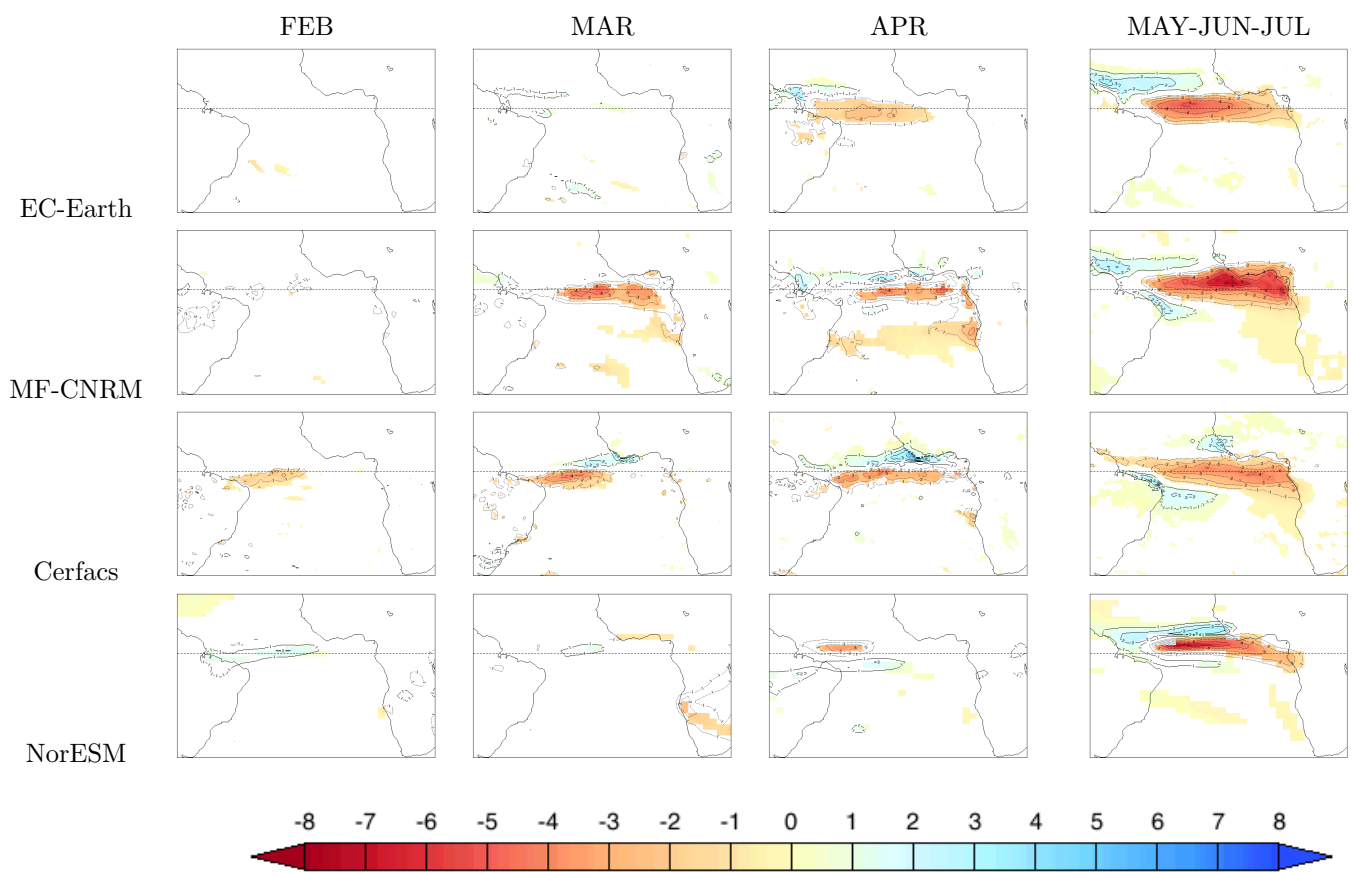


Figure 23: Precipitation (mm.d<sup>-1</sup>) difference TAU30-CTRL for February starts

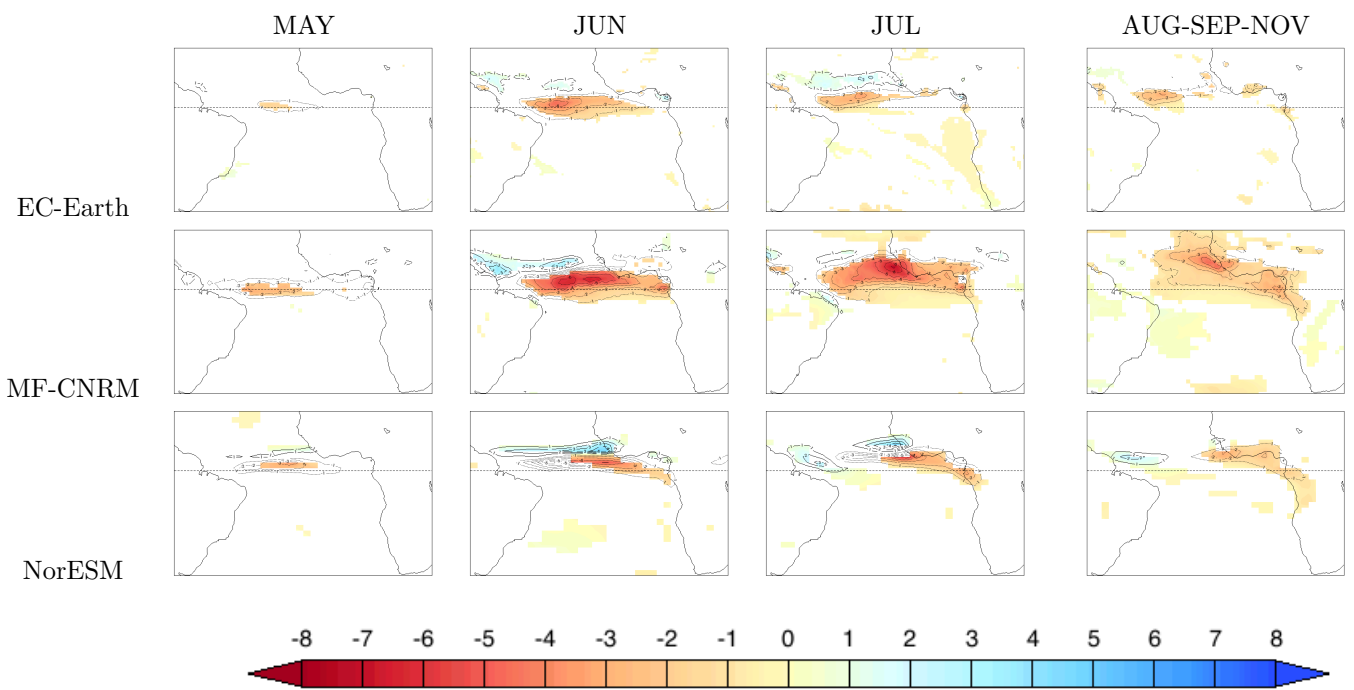


Figure 24: Same as fig 23 for May starts

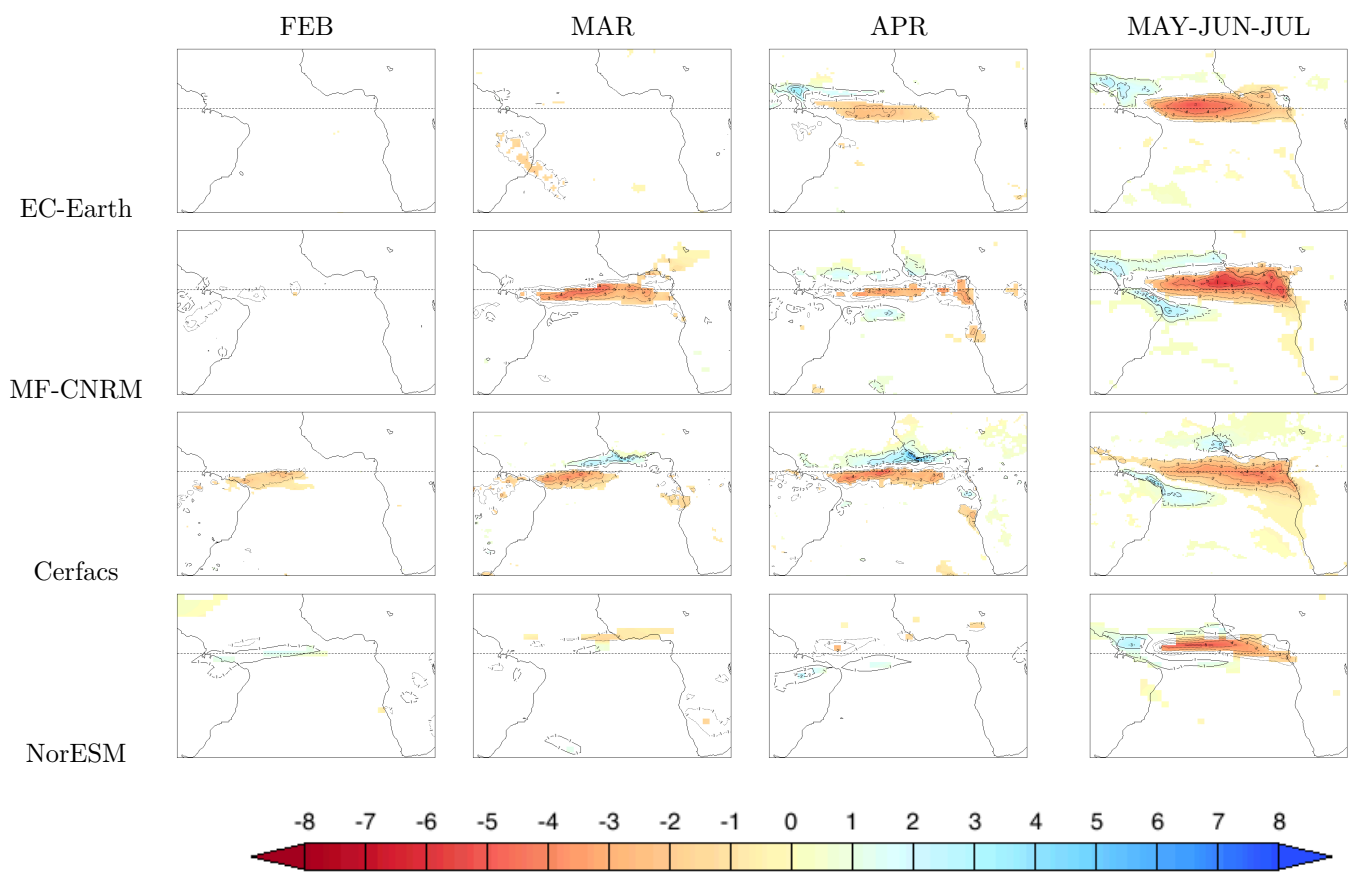


Figure 25: Precipitation (mm.d<sup>-1</sup>) difference TAUEQ-CTRL for February starts

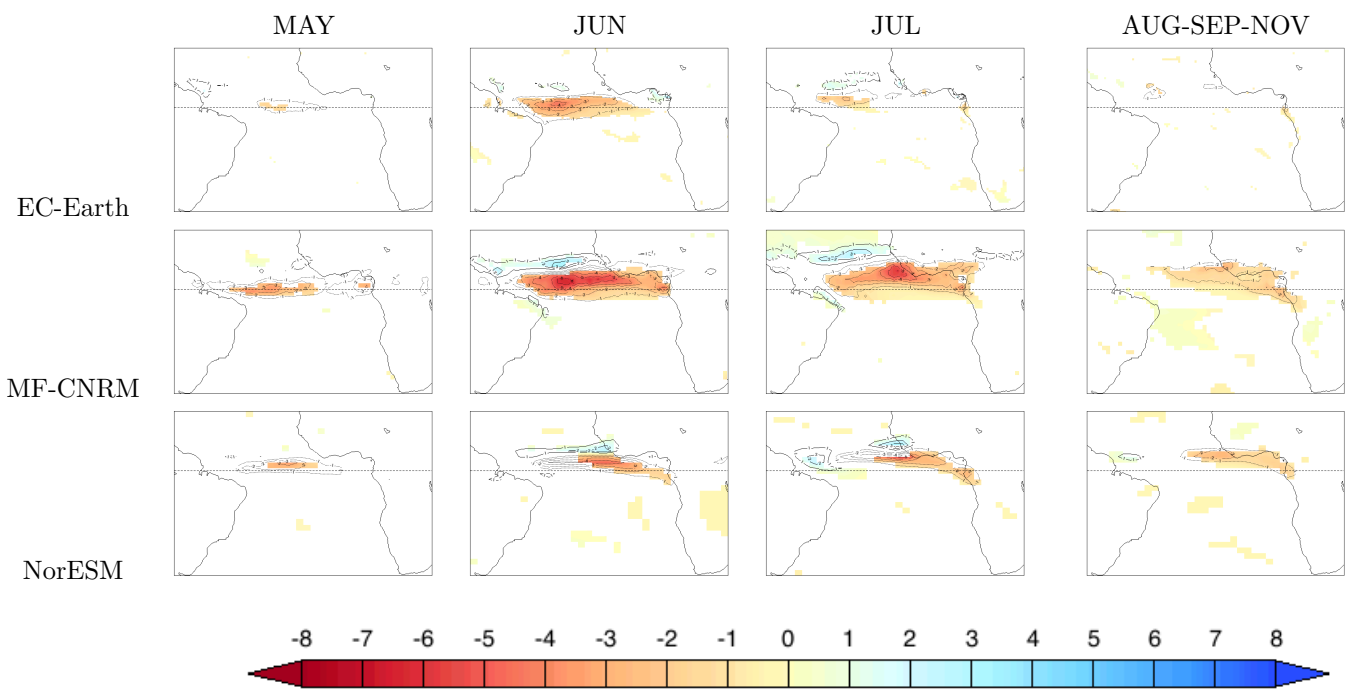


Figure 26: Same as fig 25 for May starts